NAVAL POSTGRADUATE SCHOOL
Monterey, California

19980511 167

DTIC QUALITY INSPECTED 4

THESIS

COMPUTER SIMULATION OF A TWO-PHASE CAPILLARY PUMPED LOOP (CPL) USING SINDA/FLUINT

by

Peter J. Ryan, Jr.

December, 1997

Thesis Advisor: M. D. Kelleher

Approved for public release; distribution is unlimited.

REPORT DOCUMENTATION PAGE		Form Approved OMB No. 0704-0188

Public reporting burden for this collection of information is estimated to average 1 hour per response, including the time for reviewing instruction, searching existing data sources, gathering and maintaining the data needed, and completing and reviewing the collection of information. Send comments regarding this burden estimate or any other aspect of this collection of information, including suggestions for reducing this burden, to Washington Headquarters Services, Directorate for Information Operations and Reports, 1215 Jefferson Davis Highway, Suite 1204, Arlington, VA 22202-4302, and to the Office of Management and Budget, Paperwork Reduction Project (0704-0188) Washington DC 20503.

1. AGENCY USE ONLY *(Leave blank)*	2. REPORT DATE **December 1997**	3. REPORT TYPE AND DATES COVERED **Master's Thesis**	
4. TITLE AND SUBTITLE **COMPUTER SIMULATION OF A TWO-PHASE CAPILLARY PUMPED LOOP (CPL) USING SINDA/FLUINT**		5. FUNDING NUMBERS	
6. AUTHOR(S) Peter J. Ryan, Jr.			
7. PERFORMING ORGANIZATION NAME(S) AND ADDRESS(ES) Naval Postgraduate School Monterey CA 93943-5000		8. PERFORMING ORGANIZATION REPORT NUMBER	
9. SPONSORING/MONITORING AGENCY NAME(S) AND ADDRESS(ES)		10. SPONSORING/MONITORING AGENCY REPORT NUMBER	
11. SUPPLEMENTARY NOTES The views expressed in this thesis are those of the author and do not reflect the official policy or position of the Department of Defense or the U.S. Government.			
12a. DISTRIBUTION/AVAILABILITY STATEMENT Approved for public release; distribution is unlimited.		12b. DISTRIBUTION CODE	

13. ABSTRACT *(maximum 200 words)*

The heat transfer performance of a prototype capillary pumped loop (CPL) test bed from the U.S. Air Force Phillips Laboratory is modeled using numerical differencing techniques. A commercial computer code was used to create the model and simulate performance over a wide range of operating conditions. Steady-state and transient performance were modeled as part of the initial phase of testing in a program designed to evaluate the effectiveness and reliability of capillary pumped loop technology for use in spacecraft thermal control. The performance baseline developed in this phase of testing will serve as the foundation for continued research and development of this technology.

14. SUBJECT TERMS: Capillary Pumped Loop (CPL), Evaporator, Noncondensible Gas (NCG) Trap			15. NUMBER OF PAGES **136**
			16. PRICE CODE
17. SECURITY CLASSIFICATION OF REPORT Unclassified	18. SECURITY CLASSIFICATION OF THIS PAGE Unclassified	19. SECURITY CLASSIFICATION OF ABSTRACT Unclassified	20. LIMITATION OF ABSTRACT UL

COMPUTER SIMULATION OF A TWO-PHASE CAPILLARY PUMPED LOOP (CPL) USING SINDA/FLUINT

Peter J. Ryan, Jr.
Lieutenant, United States Navy
B.S., United States Naval Academy, 1991

Submitted in partial fulfillment of the
requirements for the degree of

MASTER OF SCIENCE IN MECHANICAL ENGINEERING

from the

NAVAL POSTGRADUATE SCHOOL
December, 1997

Author: _____
(Peter J. Ryan, Jr.

Approved by: _____
Matthew D. Kelleher, Thesis Advisor

_____
Terry R. McNelley, Chairman
Department of Mechanical Engineering

iii

ABSTRACT

The heat transfer performance of a prototype capillary pumped loop (CPL) test bed from the U.S. Air Force Phillips Laboratory is modeled using numerical differencing techniques. A commercial computer code was used to create the model and simulate performance over a wide range of operating conditions. Steady-state and transient performance were modeled as part of the initial phase of testing in a program designed to evaluate the effectiveness and reliability of capillary pumped loop technology for use in spacecraft thermal control. The performance baseline developed in this phase of testing will serve as the foundation for continued research and development of this technology.

TABLE OF CONTENTS

ACKNOWLEDGMENT

I.   INTRODUCTION

A.   BACKGROUND

Most spacecraft thermal control designs use passive measures to control component temperatures. In these cases, heat dissipation requirements are easily handled by appropriately sizing an optical solar reflector (OSR) covered radiator to reject the unwanted heat out into space. These cold-biased designs employ heaters to protect more sensitive components against the extremely low temperatures encountered during periods of eclipse. These simple but effective systems have a rich flight history and are still very useful. [Ref. 1]

In the past five to ten years, the technological explosion in the areas of electronics and integrated circuitry have had a profound impact on satellite design. Smaller, faster, more powerful computers have dramatically increased the amount of data which satellites can collect, store, process, and downlink. The decreased size and weight of electronic components has allowed more hardware to be placed onboard a particular satellite bus, thereby increasing the mission capacity of each satellite.

Unfortunately, these same advances have created new challenges for the thermal control engineer. The powerful, compact electronic components dissipate considerably more heat over a smaller area. In addition, some of the more highly advanced electronics and sensors aboard modern spacecraft require cryocoolers to maintain extremely low operating temperatures. This tasks the thermal control subsystem to handle large amounts of heat rejection over long periods of time. To date, advances in spacecraft power

1

generation and thermal control systems have not been nearly as dramatic as those in the area of integrated circuit technology. The need to reliably dissipate large quantities of heat while using a minimal amount of power has sparked new interest and research in the area of satellite thermal control.

In the vacuum of space there is no medium present to accommodate heat transfer by conduction or convection to or from the spacecraft's environment. The only effective method of heat transport is by thermal radiation. Some of the more prevalent heat sources for spacecraft include onboard electronics, the sun, the earth (both by reflecting solar radiation and its own emission), thrusters, and chemical reactions. [Ref. 2]

Modern spacecraft require a diverse complement of onboard equipment to perform their missions successfully. To maximize spacecraft performance and capability while minimizing the size and cost of the launch vehicle used to get it into orbit, components are tightly packed within the spacecraft bus. As Table 1.1 shows, different components often require different temperatures to function properly. Within the satellite bus, components with significantly different operating temperatures must often be mounted in close proximity to one another. The thermal control challenge is to effectively route heat addition and removal so that the temperature integrity of each component is maintained within specifications.

Equipment	Operating Temperature (°C)
Electronics	-18 to 55
Batteries (average)	-1 to 10
Propulsion tanks and lines (Hydrazine)	5 to 49
Precision optical equipment	21 +/- 1
Solar Arrays	-130 to 75

Table 1.1 Spacecraft Component Operating Temperatures. "From Ref. [2]."

An emerging technology that has shown considerable promise for spacecraft thermal control is the capillary pumped loop (CPL). The CPL is a two-phase heat transfer loop that uses one or more capillary structures (wicks) in concert with heat addition to generate the pressure gradient which forces the working fluid to circulate from the region of heat addition to a heat rejection radiator. The heat input alone provides the energy needed to produce this pressure gradient, and thus ideally no external power input to the system is required. Although still under development, CPL technology shows significant potential for use in advanced spacecraft thermal control, where high heat transfer rates must be sustained over relatively long distances.

The Earth Observing System A.M. (EOS-AM) and the Commercial Experimental Transporter (COMET) are the first satellites designed to use capillary pumped loops as their primary thermal control system. The EOS-AM satellite is one of a series of NASA/NOAA satellites that will be studying the earth's atmosphere. The COMET satellite was designed to serve as an experimental test platform for a wide variety of space experiments. The ability of CPLs to maintain a relatively constant temperature over a wide range of heat inputs makes them especially useful for dissipating heat from cryocoolers used to cool focal planes on sensors and scientific instruments aboard these two satellites. [Ref. 3]

B.   HEAT PIPES VERSUS CAPILLARY PUMPED LOOPS

The concept and design of capillary pumped loops are similar to those of conventional heat pipes except that in the CPL system the vapor and liquid flows are in the same direction and are physically separated from each other. [Refs. 1, 2, 3]

3

Heat pipes are currently used in numerous satellite, aviation, and other mechanical thermal control systems. They have the ability to receive heat at one end and dissipate it at the other, and can control the area available for heat exchange. Vapor generated by heat input at the evaporator end travels through the inner core to the condenser end where heat is removed. There the liquid reenters the wick and capillary pumping action forces it back to the evaporator section. Basic heat pipe construction consists of a rigid container, usually cylindrical, which contains the wick structure and both liquid and vapor phases of the working fluid. Figure 1.1 shows typical heat pipe layout and operation. [Refs. 4 and 5]
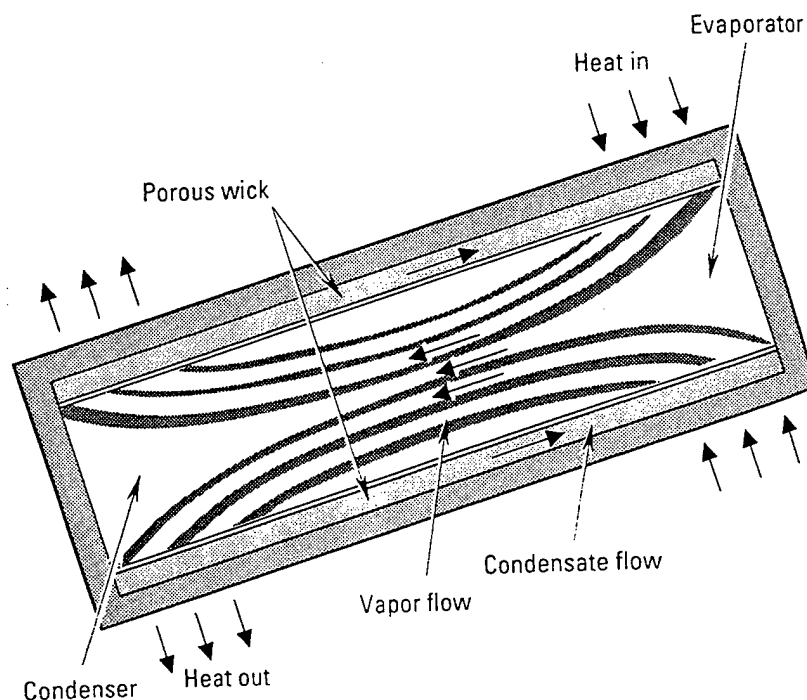
Figure 1.1 Typical Heat Pipe Layout and Operation. "From Ref. [4]."

The advantage of using capillary pumped loop systems instead of conventional heat pipes stems from the separation of the liquid and vapor phases of the working fluid. By separating the liquid and vapor portions of the heat exchanger, the heat addition and removal locations may be separated by relatively large distances. Phase separation also allows slight superheating of the vapor in the evaporator and subcooling of the liquid in the condenser, thereby increasing the system ΔT and the total heat transport capacity. Capillary pumped loops have been developed which are capable of transporting 25 kilowatts of heat over a ten-meter distance [Ref. 3]. This heat transport is over an order of magnitude greater than heat transport available with current heat pipe technology. [Refs. 2, 3, 4 and 6]

Capillary pumped loops also provide flexibility in the path in which heat is removed. The transport lines connecting the evaporator to the condenser may be routed around sensitive equipment, reducing the risk of damage or degradation from unwanted heat transfer. In addition, the CPL design provides the capability to route the condenser lines to several different radiators. Analogous to current flow in an electrical circuit, more heat will naturally flow along the path or paths with the greatest potential (temperature) difference as long as the path resistances are equal. The CPL system will automatically "select" the most efficient radiators (i.e., the ones with the least incident sunlight and therefore lowest temperature) to dissipate the acquired heat. The technology exists to make the transport lines from flexible tubing which may be attached to a deployable radiator, allowing the radiator to be positioned as required for maximum heat dissipation. [Ref. 3]

Electrical power is a precious commodity in space. To date, the best electrical generation systems are only 15-30% efficient. Degradation of these systems due to radiation effects throughout the life of the satellite reduces their efficiency even further [Ref 8]. Power is often the life-limiting design parameter, and reducing electrical power consumption is also a major satellite design goal. What makes capillary pumps attractive for thermal control is that ideally they do not require external power to force liquid through the system. The capillary action of the wick material inside the evaporator is enough to sustain the pressure gradient that forces the working fluid to circulate through the loop. The pumping process is similar to that of wax being drawn through the wick of a lighted candle or water being drawn from the roots to the top of a large tree [Ref. 4]. Lubrication, excessive wear and vibration, inertia effects caused by pump rotation, and life-cycle fatigue are some of the design challenges that can be eliminated since the capillary pumped loop has no moving parts.

The following description of CPL operation is provided to give the reader a basic understanding of the heat transport process. When sufficient heat is applied to the capillary pump (or evaporator), liquid on the outer surface of the wick material evaporates. As this working fluid changes phase, it absorbs the latent heat of vaporization and exhibits heat transfer coefficients on the order of 2,500-9,000 W/m^2K. The expanding vapor travels through the loop to the condenser. Upon reaching the condenser, the vapor begins to condense along the walls of the condenser tubes. Ideally, by the time the working fluid exits the condenser it is in the form of a subcooled liquid. The liquid exiting the condenser flows onward to supply the inner annulus of the evaporator, completing the

cycle. By regulating the amount of the condenser "open" for heat rejection, the CPL can perform as a variable conductance heat transfer device. As power input is increased, the entire condenser will eventually fill with vapor, and the CPL will no longer be able to increase conductance. This constant conductance mode represents the maximum theoretical capacity of a particular capillary loop. Figure 1.2 shows a functional schematic of a capillary pumped loop. [Refs. 3, 6, 7, 9]
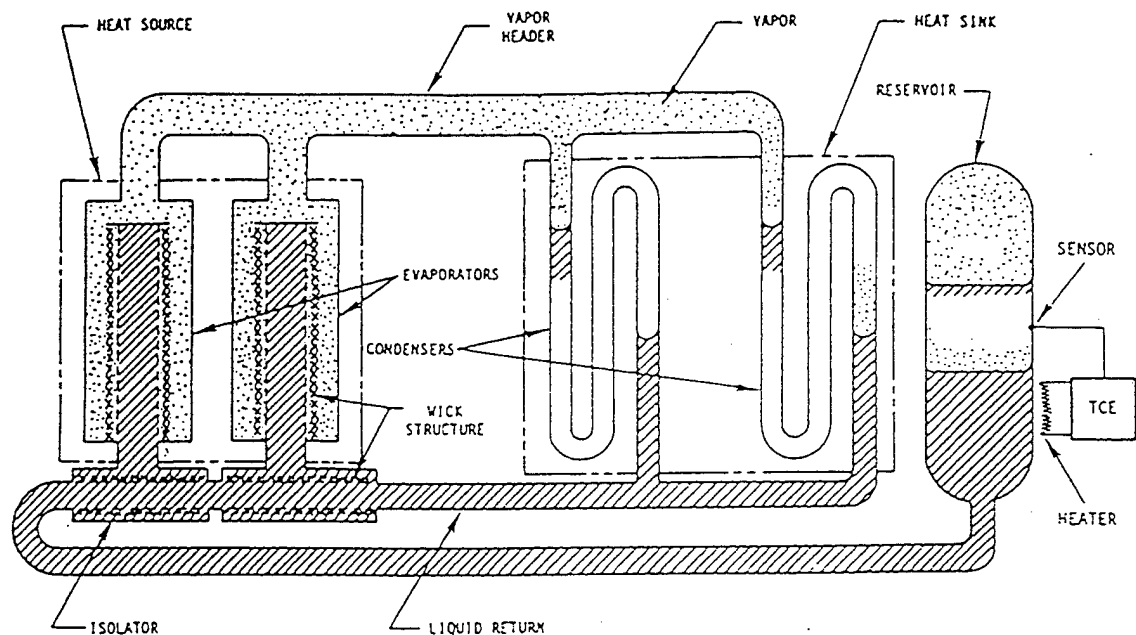
Figure 1.2 Capillary Pumped Loop Functional Schematic. "From Ref. [9]."

C. HISTORICAL SUMMARY

The first capillary pumped loop was designed and built by F. Stenger of NASA Lewis Research Center in the early 1960's [Ref. 10]. Although he published his results in 1966, it was not until the late 1970's that serious development of CPL technology began

in the West, when major aerospace corporations such as TRW, Dornier, Martin Marietta, and GE Astrospace began researching CPL technology. Universities and research institutions also began to explore both the terrestrial and space applications of CPL technology. NASA Goddard Space Flight Center (NGSFC) in Greenbelt, Maryland, has been the primary researcher in the U.S., producing CPL-1, CPL-2 and the Instrumented Thermal Test Bed (ITTB). The United States Air Force Wright Patterson Laboratory and Phillips Laboratory have also made contributions to the study of CPL and loop heat pipe technology. [Refs 8, 9, 10, 11]

In the mid 1980's, two American CPL flight experiments were conducted. The first was called (CPL/GAS), and was launched as a "Hitchhiker" experiment on the "Get Away Special" bridge in the space shuttle cargo bay in 1985. The experiment used two parallel heat pipes to dissipate 200 watts over a distance of one meter. In 1986, in a similar experiment, a refurbished CPL/GAS was flown and demonstrated the ability to transport a heat load of 500 watts. In addition to American flight tests, the Lavochkin Association of the former Soviet Union conducted a flight test on the Granat mission using a form of CPL called the Loop Heat Pipe (LHP). The Russian interest in CPL technology, which began as an effort to cool missile components, has now expanded to satellite thermal control. The Russian CPL consisted of a single evaporator that used sintered metal wicks in conjunction with a closely coupled reservoir (compensation chamber) and a single condenser. The experiment used radiant heating for evaporator heat input and was reported to be a success. The European Space Agency (ESA) and the Japanese have also conducted CPL testing. The experiments and flight tests described

above have proven the CPL concept as a viable thermal control device. [Refs. 3, 6, 7, 9, 11, 12]

In recent years, two additional flight experiments were conducted by NGSFC aboard space shuttle missions STS-60 and STS-69. The first flight experiment, CAPL-1, was conducted in February 1994 using the CPL Engineering Model One (CPL1). Over a period of eight days, twenty-one attempts were made to start four parallel evaporators. None of the startup attempts were fully successful, with only ten of the attempts succeeding in starting at least two evaporators. The experiments showed that the evaporators had a difficult time initiating nucleate boiling in the liquid-filled vapor grooves, which eventually led to deprime. [Refs. 3, 6, 9, 12, 13]

After several design changes and further ground testing, NGSFC developed CPL Engineering Model Two (CPL2), a prototype of the EOS-AM thermal control system. CPL2 was a three-port single evaporator, usually called a "starter pump". After hardening the new capillary pumped loop in a thermal vacuum chamber, NGSFC was ready to conduct another flight test. The CAPL-2 experiment was launched in September 1995 from Cape Canaveral, Florida aboard the Space Shuttle Endeavor. The flight test incorporated real time control and data acquisition, a major improvement over CAPL-1. Testing during the 198 hours of system operation included eleven startup tests, power cycling, reservoir and condenser temperature changes, recovery from three induced deprimes, and performance under small gravitational acceleration (provided by shuttle thrusters). The flight test was very successful, and proved that single evaporator, starter pump configured CPL technology is applicable to operation in a zero gravity environment.

9

Although these two experiments greatly increased the CPL flight performance database, in doing so they raised a number of new questions concerning various aspects of CPL performance. [Refs. 3, 6, 9, 13]

Despite the success of the CAPL-2 experiment, the aerospace industry still views CPL technology with some skepticism. Before full acceptance of the CPL concept, industry requires a larger flight test database, especially of multiple evaporator systems. However, in order to generate that database, CPLs must be flown as "extra" hardware on board other satellites or the space shuttle. Launching an unnecessary thermal control system just for testing is expensive, and industry currently seems content to continue using available systems and technology. Another factor that has affected the acceptance of CPL technology is that they are currently viewed as large, passive, experimental heat transfer systems for dissipating very large heat loads. Although CPLs are capable of transporting kilowatts of heat, they are equally effective at transferring much smaller amounts. Lastly, there are still a number of CPL performance phenomena that are not fully understood. Startup anomalies, transient behavior during power cycling, noncondensible gas effects, and unexplained deprime during steady state are some of the uncertainties in CPL behavior which drive the need for more ground testing. [Refs. 9, 14]

D.   OBJECTIVES

Nichols Research Corporation in association with the United States Air Force Phillips Laboratory has begun testing a prototype capillary pumped loop test facility at Kirtland Air Force Base in Albuquerque, New Mexico. The CPL testing is being conducted by the Thermal Bus Focused Technology Area (FTA) of the Phillips

Laboratory VTVS-Structural Systems Branch. The CPL test bed at Phillips Laboratory, which uses ammonia as the working fluid, was manufactured by Swales & Associates, Inc. formerly OAO Corporation, under contract from the USAF. [Ref. 9]

The Phillips Laboratory CPL test bed provides the capability to test numerous component configurations over a wide range of input parameters as well as different component orientations and elevations. The latter is important in attempting to simulate the space environment during ground testing. While it is still impractical to ground test capillary loops in a zero-g environment, adverse orientations may be tested to provide a "worst case" operational scenario. If the system can continue to perform under the imposed hostile orientations, then it will most likely survive the gravitational accelerations during launch and orbit maneuvering, and continue to perform in a gravity free environment.

The CPL test plan at Phillips Laboratory consists of four phases. Phase 'A' is a baseline characterization designed to define the basic characteristics of the Swales capillary pumped loop. This phase, which is currently underway, consists of varying reservoir and condenser temperatures, power cycling, elevation and tilt changes, and variations in startup procedure. Phase 'B' will focus on special characterization and performance improvement. Tests include using nucleation heaters on evaporator pumps instead of a starter pump, condenser heat load sharing, and reservoir cold shock testing. Phase 'C' will incorporate new components and begin design qualification. In particular, evaporator pumps of various sizes and materials, advanced wick designs, and smaller reservoirs with internal baffling are expected to be tested. During this phase, actual

equipment may be used instead of heaters to provide thermal mass to the system. Phase 'D' will be devoted to design optimization issues such as weight reduction and decreased startup time. [Ref. 9]

The purpose of this study is to develop accurate steady-state and transient models of the Phillips Laboratory capillary pumped loop using a commercial computer code. The models will increase understanding of the baseline CPL performance, will allow for augmentation with additional components, and will facilitate evaluation of component and system modifications during the latter stages of the test plan.

II. PHILLIPS LABORATORY CAPILLARY PUMPED LOOP

A.   TEST BED SETUP

The CPL test bed at Phillips Laboratory consists of three sections: the evaporator section, the transport section, and the condenser section. The evaporator section is currently made up of six capillary pumps (evaporators) with space available for two more. The transport section contains both the liquid and vapor transport lines, as well as the reservoir and the mechanical pump. The condenser section contains two parallel condensers which may be operated together or separately. The CPL test bed layout is shown in Figure 2.1. [Ref. 9]

The Phillips Laboratory CPL includes a reservoir which is plumbed directly to the starter pump, isolators, liquid and vapor transport lines whose lengths can be set at 10 feet (3.048 m), 16 feet (4.877 m), 20 feet (6.096 m), and 26 feet (7.925 m), noncondensible gas traps, and two condensers. A variable speed micropump is also installed to facilitate ground testing. The pump, which is capable of providing a flow rate of 0.5 gallons per minute at 15 psi pressure differential, may be used for repriming the system or reducing the time required for startup. The pump is only test equipment and is not required for CPL startup or operation. [Ref. 9]

To facilitate configuration changes and equipment modifications, each section of the CPL is mounted on rails attached to an aluminum base. The base structure also contains a jack which can be used to change component elevation of both the evaporator and condenser sections to $\pm$ 15 inches (0.381 m) from the normal horizontal layout of the CPL test bed. In addition, the condenser and evaporator sections may be rotated $\pm$ 60°

13

and the reservoir may be rotated $\pm$ 90°. The CPL is contained within a 182 by 44 by 84 inch (4.623 by 1.118 by 2.134 m) envelope and can be operated over a temperature range of 0 to 50°C. The test bed sits within a Lexan enclosure which is equipped with an ammonia sensor and two large ventilation fans that are activated automatically in the event of an ammonia leak. [Ref. 15]

The CPL data acquisition system is made up of a Bernouli drive, a temperature scanner to manage the thermocouple data input, and two Macintosh computers to run the Lab View software. There are 116 type T thermocouples attached to the various sections of the capillary pumped loop, with five of them being internally mounted. There is a Sensotec Model G absolute pressure transducer installed on the reservoir outlet line, and five Sensotec Model Z differential pressure transducers to measure system pressure losses in each section. Standard sampling time is three and fifteen seconds for pressure and temperature data respectively; however these may be reduced to 0.6 and three seconds respectively during startup or transient events. A schematic of the Phillips Laboratory CPL is provided in Figure 2.2.

Each evaporator pump is bolted to the bottom of an aluminum plate with a graphite foil interface to reduce the overall contact resistance and enhance heat transfer. Electric strip heaters attached to the upper side of the heater plate provide a heat input of up to 600 watts for each of the 30-inch (0.762 m) evaporators and 300 watts for each of the 15-inch (0.381 m) evaporators. Due to additional losses in the parallel evaporator configuration, the total system capacity is less than the sum of the individual evaporator heat transport ratings. The total system heat transport capability is rated at 2500 watts.

Dimensions of the Phillips Laboratory capillary pumped loop components are provided in

Table 2.1.
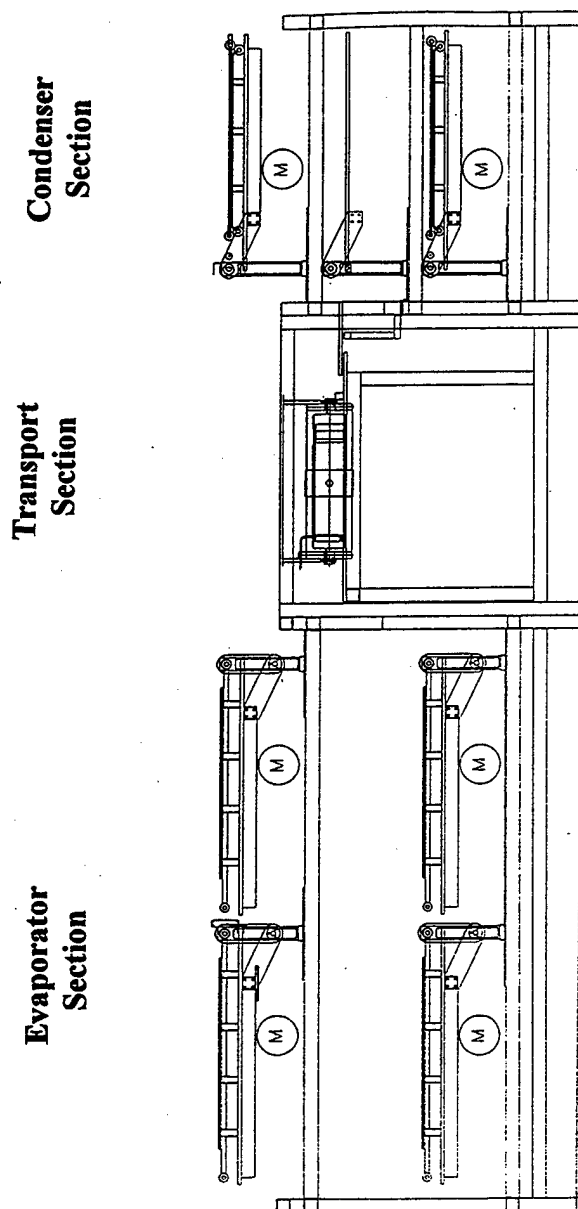
Figure 2.1. Phillips Laboratory CPL Test Bed Layout. "From Ref. [9]".
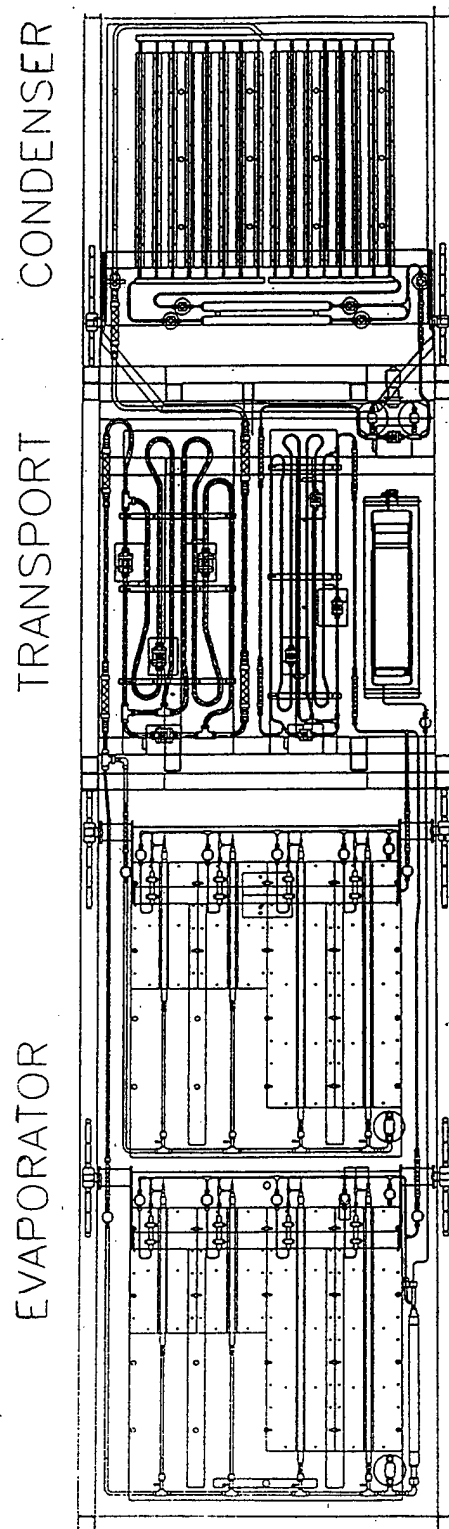
Figure 2.2. Phillips Laboratory CPL Test Bed Schematic. "From Ref. [9]."

Component	Material	Length (cm)	Inner Diameter (cm)	Outer Diameter (cm)
Reservoir	6063-T6-Al	45.72	9.930	11.43
Reservoir Connect Line	304L SS	200.4	0.216	0.318
Liquid Inlet Header	304L SS	133.5	0.457	0.635
Liquid Transport Line	304L SS	313.2	0.457	0.635
Vapor Exhaust Header	304L SS	169.1	1.021	1.270
Vapor Transport Line	304L SS	311.9	1.021	1.270
Evaporator Tubes (30 in.)	6063-T6 Al	76.20	1.384	1.600
Evaporator Tubes (15 in.)	6063-T6 Al	38.10	1.384	1.600
Evaporator Isolators	304L SS	5.080	1.092	1.270
Condenser Inlet Line	304L SS	1.528	1.021	1.270
Condenser Outlet Line	304L SS	1.750	0.457	0.635
Condenser Inlet Header	6063-T6 Al	38.74	1.422	1.905
Condenser Outlet Header	6063-T6 Al	39.21	1.166	1.905
Condenser Tubes	6063-T6 Al	73.31	0.318	0.633

Table 2.1. Phillips Laboratory CPL Dimensions.

B.   RESERVOIR

The function of the reservoir assembly in the capillary pumped loop is to control the system operating temperature, independent of the surroundings or the heat load applied. The saturated, two-phase reservoir provides for management and distribution of the working fluid. It is the relationship between the reservoir and the condenser that regulates the variable conductance of a capillary loop. Pressure differences caused by variation in heat load will vary the liquid distribution between the condenser and the reservoir. The amount of heat dissipation in the condenser depends on the "open" length, and is controlled by this liquid distribution. "Open" means that the passage is not blocked by liquid, thereby allowing vapor to enter and condense. Reservoirs are normally-cold biased, meaning that heat is required to maintain the desired set point temperature. Strip

heaters are used at Phillips Laboratory to maintain the reservoir set point temperature to within ± 2 C. [Ref. 9]

Reservoir sizing and system priming are important to CPL performance. At the cold startup condition, when most of the loop will be hard filled with liquid, there needs to be some liquid still left in the reservoir. Alternately, at high power and high set point temperature, the large amount of vapor that is generated will displace liquid from the condenser and into the reservoir. The reservoir must also be capable of handling this increase in liquid inventory. The Phillips Laboratory reservoir is designed so that it will be 11% full at the 0 C fully flooded (startup) condition and 89% full at the 50 C maximum temperature operating condition. [Ref. 9]

C.   WICK STRUCTURES

Wicks are the most important components in the capillary pumped loop system. They are found in all evaporators, isolators, and gas traps, as well as the reservoir. Selecting the wick material is one of the many design decisions that have to be made. The ideal wick would have an extremely small pore size, good permeability, and low thermal conductivity. Since pore size and permeability requirements often conflict with each other, the final selection is more of a compromise between the two.

Metal wicks offer uniformity in construction, durability, and can exhibit adequate permeability with extremely small pore sizes (down to one micron). They are easy to install and are capable of performing over a wide temperature range. American firms have just recently begun production of metal wicks, and they are still relatively expensive. Plastic wicks also have attractive pore size versus permeability characteristics and offer a

18

much lower thermal conductivity than metal wicks. However, plastic wicks have not been fabricated below a ten micron pore size and have a relatively low melting point. This limits their heat transport capability and effective temperature range. Research is currently being conducted in development of teflon wicks. Although design is still in the early stages, these wicks have shown a four to five fold increase in capillary pumping limit over conventional plastic wicks. [Ref. 15]

The wicks used throughout the Phillips Laboratory capillary pumped loop consist of a porous, permeable, ultra high molecular weight (UHMW) polyethylene thermoplastic foam. Wick pore sizes are 15 microns for all components except for two evaporators which utilize 10-micron wicks. Two sintered metal wicks with pore sizes of 1.5 microns have also been purchased, but have not yet been installed. Table 2.2 lists wick properties for some of the Phillips Laboratory capillary pumped loop components. [Ref. 9]

Wick	Material	Pore Radius (m)	Permeability (m^2)	Capillary Pumping Limit (Pa)	Flow Conductance Factor
Starter Pump	Polyethylene	1.73 E-05	4.31 E-13	2344.2	2.30 E-12
NCG Trap	Polyethylene	3.06 E-05	1.00 E-13	1323.8	7.35 E-13
Isolator	Polyethylene	1.86 E-05	1.00 E-13	2433.9	9.67 E-14
Evaporator #4	Polyethylene	2.04 E-05	1.06 E-13	2268.4	6.76 E-13

Table 2.2. Phillips Laboratory CPL Wick Properties. "From Ref. [15]".

For the NCG trap and the isolator, the capillary pumping limit refers more to the maximum pressure they can sustain across the liquid-vapor interface to effectively block vapor transport. These devices are not designed to be "primed" in the sense that during normal operation they will have liquid on both sides of the wick material.

Wicks are typically force-fit within an axially grooved aluminum tube, such that the wick outer surface and the inside of the tube are contiguous. This creates a passage on either side of the wick to provide for a liquid-vapor interface within the wick structure. There are numerous variations in the shape of the wick itself. Some of the more common designs are shown in Figure 2.3. It is the ability of the liquid-vapor interface within the wick to withstand a pressure differential that is the key to CPL operation. During normal operation evaporation occurs on the outer surface of the wick. Near the capillary pumping limit, the liquid-vapor interface recedes into the wick, reducing the heat transfer area by as much as 50 percent. [Refs. 3, 16]

D. CONDENSER

The cooling for both of the CPL condensers is provided by a FTS Systems, Inc., model #RC311B chiller which uses two compressors in a staged configuration. The chiller working fluid, Fluorinert® FC-72, is cooled by water and its temperature can be controlled to within $\pm$ 3 C. The temperature range of the chiller is from –80 to 40 C. Maximum coolant flow through the 0.125 inch (3.18 mm) piping of each condenser section is four gallons per minute. The condenser piping is mounted to a 0.3 inch (0.762 cm) thick aluminum plate. Fixed to the other side of the plate are ammonia tubes of the same size. A thin graphite film is used to reduce the thermal contact resistance at the junctions of both sets of piping and the connector plate. Each condenser section consists of eight such tubes on either side, with FC-72 lines in a counter-flow arrangement. Each condenser is capable of providing up to 1500 watts of cooling at –50 C. [Ref. 9]

Liquid subcooling is desired in CPL systems to prevent the working fluid from reaching saturation temperature within the liquid core of the evaporator. Ironically, adequate subcooling is more critical during low power operation than it is with high heat input. The reason is that at high power, the rapid rate of evaporation and resulting pressure gradient are high enough to generate a steady flow through the system. At low power, the flow is almost stagnant, and back-conduction through the wick into the liquid core can become the dominant term. For this reason, capillary pumped loops often exhibit a low power limit in addition to a maximum heat transport capability. [Ref. 9]
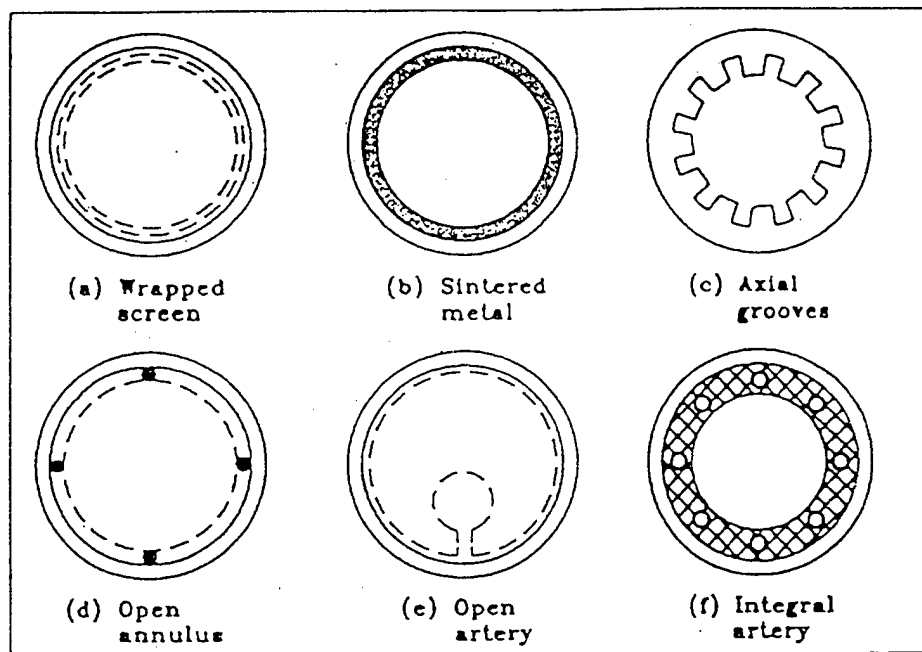

Figure 2.3. Common Wick Designs. "From Ref. [2]".

E.   NONCONDENSIBLE GAS TRAPS AND OTHER VAPOR BARRIERS

Although extreme care is taken during charging a CPL system, (i.e., filling it with working fluid) there will inevitably be a minute ingress of noncondensible gases (NCG).

is applied. This heating process or "bake-out" must be carefully done to avoid damage to wick material. In addition, during normal operation a small fraction of the working fluid itself may experience chemical breakdown. In the case of ammonia, nitrogen and hydrogen gases will be produced. Usually, the quantity of such gases is so low that their effects during normal operation are negligible. They tend to migrate through the system to the liquid cores of the evaporator pumps, where they are stopped by the wick and begin to collect. Although these gases do little to affect system performance during normal operation, their effects during power cycling can be catastrophic. [Refs. 3, 6, 7, 9, 11, 12, 16]

As power is decreased, the system pressure drops, allowing small vapor bubbles at the end of the liquid core to expand. If they grow large enough, these bubbles can block a portion of the wick surface. This reduces the area available for evaporation, and thus reduces the rate at which heat is removed from the evaporator. The associated temperature rise may expand the bubble further, blocking the entire wick surface. By destroying the liquid-vapor interface, the bubble takes away the capillary pumping force, making it impossible for the evaporator to draw liquid into its core. Heat can no longer be dissipated by this pump. This phenomenon is illustrated in Figure 2.4.

One solution to this problem is to design the evaporator core large enough to accommodate bubble formation. While this certainly makes the evaporator more robust, it also adds significant weight and cost to the CPL system. An alternative solution is to connect the outlet of each condenser to a noncondensible gas trap. The purpose of this device is to remove noncondensible gases from the liquid and prevent them from being

transported to the evaporator headers. Each NCG trap is composed of three concentric

cylinders; an outer ring, a cylinder composed of wick material, and an inner cylinder with

holes at one end. Liquid from the condenser enters between the wick material and the

Effects of Noncondensible Gases

Small NCG bubble inside evaporator liquid core. Does not create significant problems at high power.

As power is decreased, the corresponding reduction in flow rate causes pressure to decrease and core temperature to increase. This allows the bubble to grow.

Eventually the bubble will expand to the point where it blocks a portion of the wick, reducing the area available for heat transfer. The core temperature will increase, the bubble will grow further and eventually will dry out the wick causing deprime.
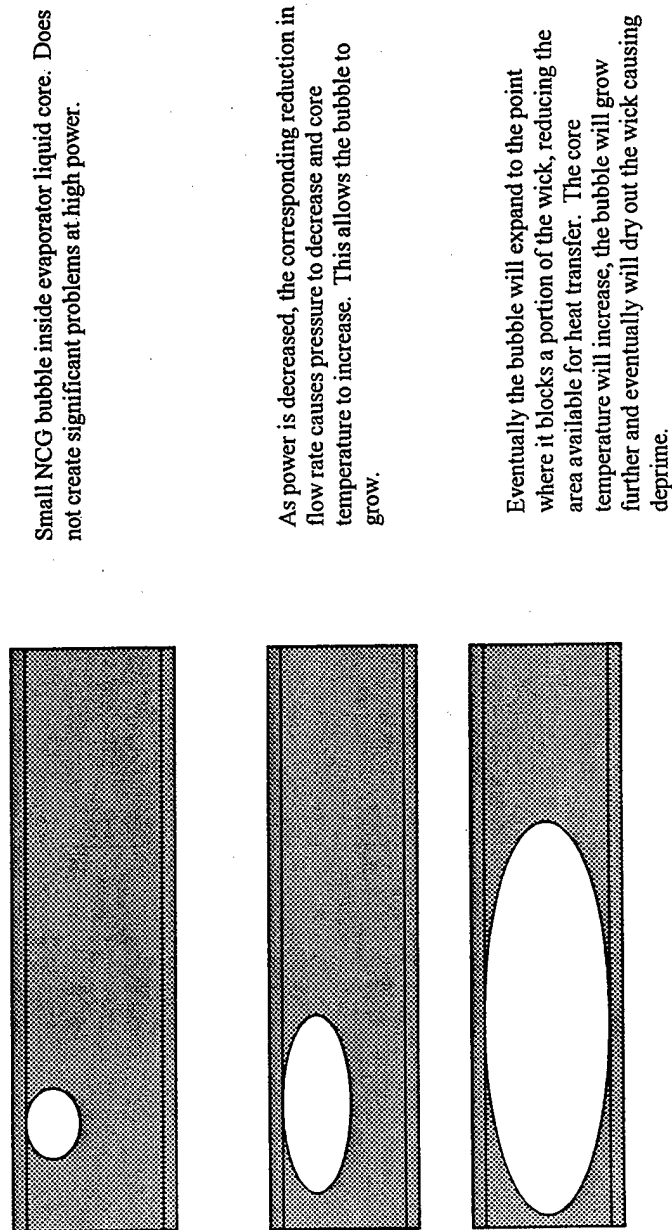
Figure 2.4. Effects of Noncondensible Gases.

inner cylinder. The wick material allows the liquid to flow through while acting as a barrier to all gas bubbles larger than its pore size. These larger gas bubbles continue to travel to the end of the trap where they pass through the holes into the inner storage area. The NCGs are placed at the subcooled outlet of the condenser because the solubility of gases in the ammonia is lowest at this point in the system. [Refs. 3, 9]

In addition to blocking the flow of noncondensible gas to the liquid transport section, NCGs also serve as flow regulators when multiple condensers are connected in parallel. Since each condenser will likely be connected to a different radiator, it is likely that each condenser will be dissipating to a different sink temperature. If the temperature of a sink (or sinks) is too high to completely condense the working fluid within that condenser, vapor will flow to the NCG, where it will become trapped. The flow resistance through the wick will force the vapor to be rerouted to another condenser. As long as other condensers are capable of handling the increased vapor flow, the ineffective condenser/radiator can be "shut down" until conditions for condensation improve. As the radiator temperature decreases, flow will gradually return to that condenser. [Ref. 3]

There are currently two basic condenser designs used in most space applications. The first design is called direct condensation and involves mounting the condenser section of the capillary pumped loop directly onto the back side of the radiator surface. This design was incorporated into most of the early ground testing and was used for the first several flight experiments. Although the design provides a very efficient and inexpensive way to transfer heat to the radiator for rejection, it is highly susceptible to micro-meteoroid bombardment. [Ref. 3]

There are over 8000 objects larger than 20 centimeters currently orbiting the earth at altitudes of 300 miles (482.8 km) or less. A ground based observatory using the Haystack Radar monitors over 140,000 objects one centimeter and larger. The average velocity of particles in these orbits is near 18,000 miles per hour. The number of these particles has increased by over a thousand in the past three years alone, and will continue to rise in the foreseeable future. Satellites, and even the space shuttle itself have had to do "evasive" maneuvers to avoid impact with orbital debris. [Ref. 17]

Some sources of this debris are spent rocket motors, accidentally lost satellite components, surface erosion, shrapnel from exploding rockets, and intentionally discarded waste [Ref. 17]. The tremendous velocities of micro-meteoroids and other orbital debris gives even minute particles enormous momentum. Although the density of these micro-meteoroids is very low and likelihood of impact even smaller, a single puncture would result in the complete loss of working fluid inventory and result in total failure of the thermal control system.

An alternative to direct condensation is the heat pipe heat exchanger (HPHX). In this design heat is transferred from the condenser to multiple heat pipes through an interface heat exchanger. This heat exchanger removes heat from the capillary loop condenser(s) and applies it to the evaporator sections of the heat pipes. These heat pipes are in turn mounted to a radiator surface, so they can reject the received heat. Although a micro-meteoroid impact may still disable one of the heat pipes, the system will not suffer degradation as long as the other heat pipes are capable of handling the increased heat load. This design is the prototype for the EOS-AM, and has performed well during ground

testing, where it demonstrated a heat exchange rate of over 800 watts and heat transfer coefficients in excess of 6000 W/m^2K. [Ref. 3]

Wicks are also used as vapor barriers in both the isolators and the reservoir. In the reservoir, which contains a two-phase mixture and is connected to the evaporator liquid headers, the wick prevents vapor from flowing to the evaporators. The isolators are relatively small, with only about 2 inches of active (wicked) length. The isolator wicks are also designed to prevent the passage of vapor. There is one isolator for each capillary pump, so that if that pump deprimes, vapor will not flow back through the liquid header and into the liquid cores of other pumps, thereby causing all pumps on that header to deprime. [Ref. 9]

F.   STARTER PUMP

The starter pump is a short evaporator pump with a relatively large diameter designed to clear vapor from the evaporator grooves of the other evaporators in the system. By clearing the vapor grooves, the starter pump creates a liquid-vapor interface in the other evaporators. With an interface present, surface evaporation rather than nucleate boiling occurs. If an evaporator is hard filled, i.e., both sides of the wick are filled with liquid, superheat is required to initiate boiling. [Refs. 3, 6, 7, 9, 16]

Superheat is undesirable for two reasons. First, when fluid in the vapor channel is superheated just a few degrees, the onset of boiling will be characterized by rapid formation of a large vapor bubble. This sudden "explosion" of vapor causes a pressure surge that could exceed the capillary limit of the evaporator pump and blow vapor back through the wick. In addition, conduction through the wick may allow the vapor channel

26

superheat to raise the evaporator core temperature above the saturation limit, allowing vapor to form in the interior of the wick. As with noncondensible gases, accumulation of vapor inside the liquid core reduces the effective heat transfer area and may cause the evaporator to deprime. [Refs. 3, 6, 7, 9, 11, 12]

Since the starter pump plays such a significant role in reliable start up of the entire CPL system, it is protected against deprime during its own startup. A device called a bayonet, which is simple an extension of the reservoir input line, is installed deep within the starter pump liquid core. With the bayonet positioned deep within the liquid core of the starter pump, cool liquid flowing into the bayonet tip will help compress, condense, or flush out any bubbles existing in the evaporator core. Liquid returning from the condenser to the reservoir must first flow through the starter pump core before flowing through the bayonet into the reservoir. [Ref. 9]

Vapor exiting the starter pump displaces liquid from the vapor line and the vapor grooves of other evaporators. To ensure grooves are cleared, a Capillary Vapor Flow Valve (CVFV) is installed in the vapor line. The CVFV is a screen which prevents the liquid/vapor interface from traveling to the condenser section until the evaporator grooves are cleared. The holes in the screen are smaller than the evaporator vapor grooves, so vapor produced by the starter pump will tend to empty the larger cavities first. [Ref. 9]

III. CAPILLARY PUMPING THEORY

A. THEORY

By definition, all liquids are in a state of tension. This tensile force comes from molecular interaction of surface molecules with adjacent ones in the fluid interior. Tensile stress in solid materials is defined as the force per unit area normal to the direction of the force. Surface tension is expressed as force per unit length along the surface. This avoids uncertainty about the actual area over which the force acts. Surface tension is a function of temperature, almost always decreasing with increasing temperature, and changes slightly with the type of gas at the liquid-vapor interface. Surface tension is fundamental to capillary pumping theory. [Refs. 4 and 5]

Another factor that plays an important role in capillary pumping theory is the cohesion or adhesion between the molecules within a certain liquid and a given surface. The term "wettability" is used to describe the relationship between the two. A liquid will "wet" the solid if adhesion dominates over cohesion. Conversely, a liquid will be non-wetting if cohesive forces between liquid molecules dominate. An accurate measure of surface wettability is the contact angle observed between a drop of liquid and the surface. As shown in Figure 3.1, wetting liquids will usually have contact angles less than 90 degrees.

Capillary effects are greatest when a liquid is either highly wetting or highly nonwetting. For this reason, most heat pipes and capillary pumped loops use liquids that are highly wetting. Ammonia is a common working fluid, because it exhibits excellent

wettability on hard, solid surfaces, is inexpensive, and does not tend to react with standard CPL and heat pipe materials such as aluminum and stainless steel.
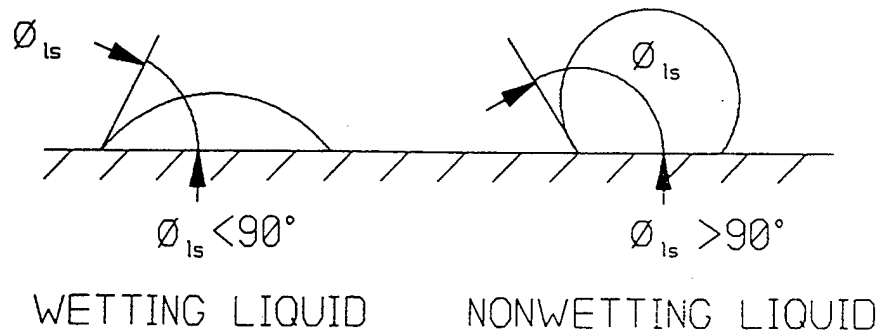
Figure 3.1. Contact Angle: Wetting and Nonwetting Fluids. "From Ref. [4]."

Capillarity is a term that describes the ability of a curved liquid surface (meniscus) to sustain a pressure differential across that surface [Ref. 4.]. This pressure differential is the driving force behind the CPL system, and determines the maximum heat transport capability. When the capillary limit of the wick material is reached, further increase in the heat input cannot be matched with an increase in flow rate. The evaporator will not be able to draw liquid into its core at the rate with which it is evaporating at the wick surface. In time the heated part of the wick will dry out, causing the evaporator to deprime.

The capillary limit for a certain wick is defined as

$$\Delta Pc = \frac{2*\sigma}{(r/\cos\phi_s)}$$

where σ is the surface tension of the liquid, r is the bubble radius of curvature, and ϕ_s is the contact angle at the interface.

The bubble radius is often difficult to measure directly, and the following alternate form is usually used.

$$\Delta Pc = \frac{2*\sigma}{r_p}$$

where r_p is the effective pore radius of the wick.

Note that the capillary pumping limit is a function of the wick pore radius, surface tension, and contact angle *only*. The length and diameter of the evaporator have no effect on the capillary pumping limit. The polyethylene wick inside Evaporator Pump No. 4 at Phillips Laboratory has a capillary pumping limit of 2268.4 Pa (0.239 psid). In order for the evaporator pump to remain operational, the sum of all the pressure losses throughout the loop must be less than this small amount. System pressure losses are mostly due to friction within the loop piping and capillary devices such as isolators, NCG traps, etc. If certain components are at different elevations, there may also be losses (or gains) from gravity. The following equation summarizes the pressure requirements for a capillary pumped loop. [Ref. 9]

$$\Delta Pc \geq \Delta P_{wick} + \Delta P_f + \Delta P_{isol} + \Delta P_g$$

In general, the pressure losses in capillary wicking structures (ΔP_{wick} and ΔP_{isol}) are functions of the liquid viscosity and the wick permeability and can be estimated by the following equation.

$$\Delta P_{wick}, \Delta P_{isol} = \frac{\mu_l * Q * D_o}{2*\pi*\lambda*K_{wick}*L_{wick}*D_i}$$

ΔP_g, the pressure loss due to gravity, may be calculated from

$$\Delta P_g = \rho*g*h$$

ΔP_f is the sum of the frictional pressure losses due to pipe flow, and can be calculated for each pipe section from

31

$$\Delta P_f \quad = \quad \frac{64 * L * V^2}{Re * D * 2}$$

Obviously, pressure losses are a major concern in CPL system design. Pipe sizing and interior surface finish are selected to minimize flow resistance within the loop. In the Phillips Laboratory CPL, all transport lines are electro-polished to achieve a surface roughness of less than 24 micro inches (0.61 μm) RMS. Fortunately, flow rates are usually well within the boundaries for laminar flow, and pipe losses are typically small. The CVFV is designed and positioned so that the wet screen is capable of blocking flow of vapor during startup without creating a large pressure drop during normal (dry) operation. Although the wick material in the isolator and the noncondensible gas traps contribute to the overall pressure drop, the important functions these devices perform warrant their associated pressure drops. [Ref. 9]

IV. DEVELOPING THE MODEL

A. SINDA/FLUINT

Although the operating principles of capillary pumped loops are relatively simple, the design of a CPL system is quite complicated. The system components are extremely interdependent and analytical modeling of these systems is almost a necessity. The Systems Improved Numerical Differencing Analyzer and Fluid Integrator (SINDA/FLUINT) is a software package which is very useful in system design and evaluation. It is a general purpose thermal/fluid simulation tool which has evolved from a thermal analysis program developed by the Chrysler Corporation in the late 1960's. Martin Marietta expanded the original program to incorporate fluid analysis as well as convection and radiation effects. [Ref. 16]

The current version of the software, SINDA/FLUINT 3.2, is currently maintained and distributed by Cullimore and Ring Technologies, Inc. NASA presently uses SINDA/FLUINT as its standard program for thermal analysis involving single and two-phase pumped thermal control loops. [Ref. 16]

Throughout this chapter program-specific terminology was used to help simplify the documentation of the CPL model development. Appendix A contains a list of SINDA/FLUINT nomenclature and terminology used in this chapter, along with a brief description of each term. Appendix B is a listing of CPL components and the corresponding SINDA/FLUINT element number(s) used to model them. The elements in the submodel diagrams may be referenced back to the exact component which they model.

SINDA and FLUINT are really two separate programs which are capable of functioning independently of one another. It is the capability to mesh the heat transfer energy balance calculated by SINDA with the one-dimensional fluid flow mass, momentum, and energy balance calculated by FLUINT that gives SINDA/FLUINT the capability to completely model complex two-phase systems. [Ref. 16]

SINDA/FLUINT is designed as a support tool, and is not very effective without sound engineering input. If the user fails to input accurate data, connect components correctly, and select the best available solution routine, the program will either abort or report a convergence failure. If a system would not work in real life, then it most likely will not work in SINDA/FLUINT either. There are no "cook book" solutions for any problem, and the user must make many decisions to come up with a model that effectively simulates system behavior while producing desired parameter data. It is up to the user to determine the scope of the model and what outputs are necessary. Not enough data makes post-processing and analysis difficult, and too much data makes the model hard to maintain and increases run time. [Ref. 16]

SINDA is a network-style (resistor-capacitor circuit analogy) simulator for heat transfer problems. Although capable of producing similar results to finite differencing or finite element programs, SINDA is actually an equation solver. This provides the user with more flexibility because unlike finite element programs, SINDA is not geometry based. The user is free to create an arbitrary network of temperature points (nodes) connected by heat flow paths (conductors) and can easily change the geometry without having to restructure the entire model. The user can select from one of the available

solution methods or write their own customized solution procedure using FORTRAN-style logic. The longevity and popularity of SINDA/FLUINT can be attributed in part to the flexibility it provides the user. [Ref. 16]

Within SINDA there are four types of nodes available for use in thermal circuit modeling. These are boundary, diffusion, arithmetic, and heater nodes. Boundary nodes have infinite thermal capacitance and may not receive an impressed heat source. Their temperature is time-independent, making them ideal for representing isothermal boundaries and sinks. Diffusion nodes have finite thermal capacitance, and thus the amount of thermal energy stored within such nodes changes with time. These are the most common types of nodes, and are applicable to almost every component or boundary within a thermal model.

Arithmetic nodes are similar to diffusion nodes, except that they have zero capacitance. The nodes are instantaneously brought into a steady state energy balance according to the heat flux supplied and heat exchange with surrounding nodes. The mass of a component modeled by an arithmetic node must be accounted for by a neighboring diffusion node. This makes it impossible to build a thermal model consisting solely of arithmetic nodes. Arithmetic nodes are useful, but their instantaneous changes can result in system instabilities and oscillations. Heater nodes are used to determine the amount of heat required (either input or output) to maintain a set temperature.

In SINDA, all thermal nodes must be connected by conductors. There are two basic types of conductors, linear and radiation. The most common category is linear conductors. Examples of linear conductors include:

1. Heat transfer by conduction

$$G = \frac{k*A}{L}$$

where k is the thermal conductivity, A is the area $\perp$ to heat flow, and L is the length of heat flow path.

2. Heat transfer by convection

$$G = h*A$$

where h is the heat transfer coefficient and A is the heat transfer area.

3. Heat transfer by advection (mass transfer)

$$G = m*Cp$$

where m is the component mass and C_p is the specific heat at constant pressure for the material.

For radiation, the conductance is input in units of energy per unit time per degree to the fourth power. The user must input the emissivity of the radiating surface, the heat transfer area, and the appropriate view factor between the control volumes exchanging energy. The Stefan-Boltzman constant is already incorporated into the program, however the user must ensure the system of units is accurate.

To facilitate modeling of heat transport by mass flow, conductors may be modeled as one-way conductors. This permits the "downstream" node to be affected by the "upstream" node, while the "upstream" node remains thermally isolated from the "downstream" node. A common type of one-way conductor is a tie, which is used to connect SINDA elements to an appropriate FLUINT element. [Ref. 16]

FLUINT is intended to provide general analysis and modeling of one-dimensional internal flow problems. As with SINDA, FLUINT is based on network methods and is geometry independent. The program is capable of steady-state and transient modeling for any fluid, and is capable of handling transitions between single and two-phase flows. The program contains a library with fluid properties for over 300 fluids, 26 of which may be incorporated into the same model. Library fluids are identified by their ASHRAE refrigerant number. In addition to the fluids available in the program library, the user has the option of inputting their own fluid properties. The program also has the capability of dealing with multiple constituent flows. [Ref. 16]

To build a fluid submodel, FLUINT uses components called lumps to create a system similar to the nodal network in SINDA. There are three types of lumps available in FLUINT. Plena are the FLUINT equivalent of boundary nodes. They have infinite volume and constant thermodynamic state. Tanks are analogous to SINDA diffusion nodes. They have finite volume and experience mass and heat transfer with resultant change in thermodynamic state. The user has an option of defining the volume of the tank in functional form, making it easy to simulate pistons, accumulators, or diastolic pumps. The fundamental tank equations used in FLUINT are:

1. Tank Mass:

$$dm/dt \ = \ \Sigma \, FR_{in} \ - \ \Sigma \, FR_{out} \qquad (FR \ = \ mass \ flowrate)$$

2. Tank Energy:

$$dU/dt \ = \ \Sigma \, (Hl_{donor} * FR_{in}) \ - \ \Sigma \, (Hl_{eff} * FR_{out} \ + \ QDOT \ - PL*(dVOL/dt)$$

3. Tank Volume:

$$dVOL/dt \ = \ VDOT \ + VOL*COMP*(dPL/dt)$$

Junctions serve the same purpose as arithmetic nodes. They contain no volume and instantly change to maintain the flow energy balance. They let the user define important points in the fluid flow path without lengthening solution time. Since junctions have no volume, the volume of the part of the system which they represent must be accounted for in an adjacent tank. Again, no fluid model may be constructed by using junctions for every lump. The basic equations for junctions are:

1. Junction Mass:

$$\Sigma \, FR_{in} \; - \; \Sigma \, FR_{out} \;\; = \; 0$$

2. Junction Energy:

$$\Sigma \, (Hl_{donor} * FR_{in}) \; - \; \Sigma \, (Hl_{eff} * FR_{out}) + QDOT \; = \; 0$$

As in SINDA, the components in FLUINT must be connected via flow paths. There are two types of paths, tubes and connectors. Tubes have finite volume and their flow rates cannot change instantly. They are useful in smoothing out transient solutions, but offer no real advantage for steady state modeling. The momentum equation for a tube is:

$$dFR/dt \; = \; (AF/TLEN)*(Pl_{up} - Pl_{down} + HC + FC*FR*|FR|^{FPOW} + AC*FR^2)$$

The other type of path is the connector. Connectors are time-independent path through which lumps may exchange energy and mass. Connectors do not model a single "real" piece of fluid hardware, and may be tailored to model a diverse group of fluid components. They may be used to represent pumps, valves, bends, orifices, and certain capillary devices (wicks). The governing equation for the kth connector is represented in FLUINT by the following:

$$\Delta FR_k^{n+1} = GK_k^n (\Delta PL_i^{n+1} - \Delta PL_j^{n+1}) + HK_k^n + EI_k^n \Delta HL_j^{n+1} + EJ_k^n \Delta HL_j^{n+1} + DK_k^n \Delta FR_k^{n+1}$$

FLUINT also has the ability to model fluid devices. Constant and variable speed pumps, check valves, control valves, heat exchangers, and evaporators may be modeled using built-in utilities. The built-in models are more complex than user built devices, taking into account fluid accelerations, phase changes, and pressure losses. [Ref. 16]

There are four built-in solution routines within SINDA/FLUINT: STDSTL, FASTIC, FORWARD, and FWDBCK. Selection of solution method depends on the type of model to be solved, the desired accuracy, and computation time available. A brief description of each solution method is outlined below.

1. STDSTL/FASTIC

These subroutines calculate the steady-state solution for both fluid and thermal networks. A successive point iterative method is used to balance the energy flows through diffusion and arithmetic nodes. One pass through all nodes is called an iteration. The heat balance for the ith node on the $k+1^{th}$ iteration is:

$$0 = Q_i + \sum_{j=1}^{i=1} [G_{ji} (T_j^{k+1} - T_i^{k+1}) + G'_{ji} \{(T_j^{k+1})^4 - (T_i^{k+1})^4 \}]$$

$$+ \sum_{j=1}^{N} [G_{ji} (T_j^{k+1} - T_i^{k+1}) + G'_{ji} \{(T_j^{k+1})^4 - (T_i^{k+1})^4 \}]$$

The superscript ($'$) on the G terms indicates that the conductance is radiative in nature. This same procedure is also used in the FASTIC, however FASTIC is more tolerant of inconsistencies in initial conditions. With both routines the user must specify the maximum number of iterations per time step as well as nodal temperature and fluid

property convergence criterion. Relaxing the criterion may help speed up the solution process. As with all solutions, the necessary benchmark for accuracy is the network energy balance. [Ref. 16]

2. FORWARD

This subroutine calculates solutions for transient problems. It uses an explicit forward differencing method to perform the thermal analysis, and implicit differencing for the fluid analysis. The heat balance equation in finite difference form is:

$$\frac{C_i}{\Delta T}(T_i^{n+1} - T_I^n) = Q_I + \sum_{j=1}^{N} \left[G_{ji}(T_j^n - T_I^n) + G'_{ji}\left\{(T_j^n)^4 - (T_I^n)^4\right\} \right]$$

where T_j^n is the temperature of node j at the current time t, and T_i^{n+1} is the temperature of node i at the next time $t + \Delta t$.

3. FWDBCK

This solution routine performs calculations for transient problems by implicit forward-backward differencing for the thermal submodels and by implicit backward differencing for the fluid submodels. A heat balance equation for a diffusion node is written as both a forward difference equation and a backward difference equation.

$$\frac{2*C_i}{\Delta t}\left(T_i^{n+1} - T_i^n\right) = 2*Q_i + \sum_{j=1}^{N} \left[G_{ji}(T_j^n - T_i^n) + G'_{ji}\left\{ (T_j^n)^4 - (T_i^n)^4 \right\} \right]$$

$$+ \sum_{j=1}^{N} \left[G_{ji}(T_j^n - T_i^n) + G'_{ji}\left\{ (T_j^n)^4 - (T_i^n)^4 \right\} \right]$$

This equation uses the average of the temperature derivatives at the current and future time steps to predict the overall temperature change. [Ref. 16]

To facilitate model production, debugging, and interpretation, Cullimore and Ring Technologies, Inc., has added a graphical user interface. The SINDA Application Programming System (SINAPS) is an extremely useful program that significantly enhances modeling capabilities. SINAPS allows the user to build a model graphically using icons to represent various components. The input blocks for each component are provided in spreadsheet format to facilitate model creation and maintenance. SINAPS feeds the input data to SINDA/FLUINT, and after the simulation has been run, reads the output file for processing. This visualization tool helps accommodate higher-order modeling and enhances pre- and post-processing operations. With SINAPS, the user can produce X-Y plots, bar graphs, and data tables of system parameters. There is also an option to color icons by temperature, quality, pressure, flow rate, heat transfer rate, and conductance. [Ref. 16]

B.   STEADY-STATE MODEL

The first step in developing the steady-state model of the Phillips Laboratory capillary pumped loop was to decide which system components were to be modeled. First, the model had to accurately reflect steady-state performance over a range of heat inputs and condenser temperature settings. Second, the model had to be well documented and well laid out so future updates could easily be made. A CPL schematic, modified to show only the portion modeled, is provided in Figure 4.1.

The first portion of the overall model to be discussed is the fluid submodel CPL2. Fluid models tend to be more complex than thermal models in that they require more input, more complex user logic, and are more likely to contain oscillations during the

solution process. For this reason, fluid modeling began with the fewest components possible, and was only added to if required for the accuracy of the solution. Since small changes in inputs, or the addition of even one more component can drastically change the model solution, additions had to be made slowly and the model had to be validated after each change.
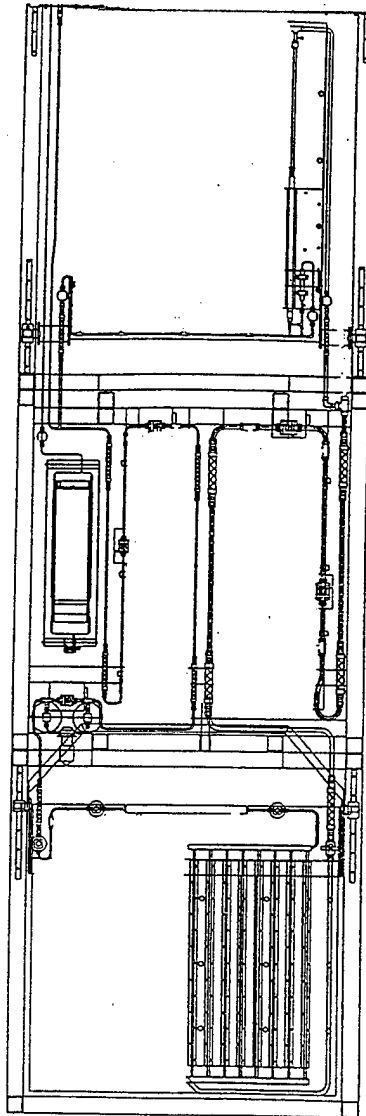
Figure 4.1. Schematic of Modeled Portion of Phillips Laboratory CPL .

The FLUINT model contains the components and flow paths required to simulate CPL operation. For the steady-state model only one evaporator pump (Evaporator pump No. 4) was selected for modeling. It has proven to be the most robust of the evaporators, and has undergone the most testing. The pump is 15 (0.381 m) inches long, and is located at the far end of the inboard evaporator plate. Since the location of this evaporator is at the end of an evaporator section, it will be relatively easy to add additional pumps at a later date. The solution procedure chosen assumed that the pump had already successfully started. This eliminated the need to model the starter pump and avoided the transient pressure surge which accompanies the clearing of the evaporator vapor grooves and the displacement of liquid from the vapor section during startup.

The reservoir is a vital component in the CPL system and was therefore included in the model. To simplify its representation, a plenum was used. Essentially this selection assumes that the reservoir is capable of perfect system temperature regulation regardless of heat input or condenser sink temperature. While this may not be true at heat inputs near maximum, previous modeling of other CPLs has shown that this assumption is valid throughout most of the CPL operating range [Ref. 16]. The reservoir pressure was set to match the experimental system operating pressure of 1.1652 MPa, and the temperature was set at the corresponding saturation temperature of 30 C. All lumps in the system were initialized to this pressure. An STUBE was used to connect the reservoir to the liquid transport line, however since there is no flow to or from the reservoir through this small diameter tube during steady-state operation, the flow rate through this STUBE was set to zero and the volume of the tube was not incorporated into an adjacent tank.

Tanks were used to account for the volume of the liquid transport line from the condenser, and the liquid header. Tank temperatures were set at 16 C, which accurately reflects the subcooling provided by the condenser. The qualities of these tanks were initialized at zero. All tanks were given a compliance of 8.85 E-09 cubic meters per Pa. The compliance allows for minute changes in tank volume and helps avoid system pressure spikes which contribute to evaporator pump deprime.

Although this seems like a misrepresentation of reality, it really isn't. Pressure oscillations during normal operation are inherent to CPL performance. At high power inputs, some short pressure spikes may reach or exceed the capillary limit of an evaporator. In testing it has been shown that the extremely short duration of the spikes is usually not enough to deprime an evaporator. Due to the analytical nature of SINDA/FLUINT however, the program "sees" the pumping limit be exceeded and deprimes the pump. [Ref. 16]

A CAPIL connector was used to connect the liquid inlet header tank with a tank representing the liquid inside the core of the evaporator pump. The CAPIL device, which models the evaporator isolator, is similar to an STUBE except the CAPIL adds the pressure loss and vapor blocking properties of the isolator capillary wick structure. Inputs to the CAPIL connector are the effective pore radius and the flow conductance factor (CFC). The CFC is a term which relates the effective flow resistance through a wick structure to the flow rate and phase of the fluid.

$$CFC = \frac{2*\pi*P_w*L}{\ln (r_o/r_i)}$$

In this equation, P_w is the wick permeability (m^2), L is the effective wick length (m) and r_o, r_i are the wick inner and outer radii.

The tank representing the evaporator liquid core was directly connected to the CAPPMP macro, and was therefore essential in maintaining the primed state. The initial tank temperature and pressure were identical to those of the liquid inlet header tank. In order for the CAPPMP to stay primed, the quality of this tank had to remain at zero.

The CAPPMP macro is a powerful built-in component which was used to model the capillary pump evaporator. The macro consists of a centered junction which is connected to adjacent fluid lumps via specialized NULL connectors, and to a different node in a thermal model via a tie. The macro is extremely useful because it takes into account the pressure drop through the wick, the pressure gradient across the liquid-vapor meniscus, and the capillary pumping limit of the wick structure. The initial temperature was set to that of the subcooled liquid and the quality was set to zero. The XVH and XVL values for the CAPPMP model were also relaxed to help maintain the primed state. The overall heat transfer conductance of 134.1 W/C was calculated using an average heat transfer coefficient of 7,000 W/m^{2}C and the outer wick surface area.

$$UA = h * \pi * D_o * L$$

D_o and L are the outer diameter and active wick length in meters. The CAPPMP macro is directly tied to a diffusion node in the EVP thermal submodel which represents the evaporator tube wall. The tie is the path through which heat from the heater element flows to the evaporator.

Although the evaporator wick is made of polyethylene, there will still be a small amount of conduction through the wick to the evaporator liquid core. If the wick is sufficiently wet, there will also be conduction through the ammonia itself. Several

45

modifications were made to the steady-state model to account for back-conduction through the evaporator wick. The first alteration was the addition of an arithmetic node to the EVP submodel, to which the CAPPMP tie was connected. The purpose of the arithmetic node was to accurately represent the saturation temperature. To do this, the normal evaporator UA coefficient was multiplied by 100, making it large enough to provide minimal temperature difference without affecting problem stability. A conductor with the old value of UA as its conductance completed modification by connecting the evaporator wall node to the saturation node. [Ref. 16]

To simulate back-conduction, the tank representing the evaporator liquid core was thermally tied to the saturation node. The UA coefficient was calculated using

$$UA = \frac{2*\pi*k_c*L}{\ln(r_o/r_i)}$$

Where k_c is the average conductivity and is obtained from

$$k_c = \varepsilon*k_{liq} + (1-\varepsilon)*k_{wick}$$

The ε in the above equation is the fraction of the wick that is wetted.

In addition to back-conduction through the wick, generated vapor will come in contact with the evaporator wall during its transit through the evaporator grooves. Since the evaporator wall temperature is above the saturation temperature, a small degree of sensible heat will be added to the exiting vapor. In an attempt to model this superheat, a junction was added to represent the vapor grooves in the evaporator. This junction was thermally tied to the evaporator wall node to provide a path for the superheat. The UA coefficient for this tie was derived from the groove are and average film coefficient, both

of which were provided by the manufacturer.

To connect this junction to the junction representing the evaporator exhaust header, an STUBE was used. Since vapor is generated all along the length of the evaporator, using the entire length would overestimate the true vapor path length. For this reason, the length of the STUBE was set to the half-length of the evaporator. The hydraulic diameter and the flow area per groove were obtained from the manufacturer, and duplication factors of 26 were used on both the upstream and downstream ends to account for the 26 grooves in the TAG 19 evaporator. [Refs. 9, 16] A diagram of the thermal resistance network for the CPL model is provided in Figure 4.2.

As in real life, evaporator pumps in the model are temperamental, and it is difficult to model steady-state without encountering evaporator deprime. Several programming methods were used to help prevent evaporator deprime. The first method involved the inputs to the XVH and XVL blocks of the CAPPMP macro. The terms represent the quality of adjacent lumps necessary to sustain the pump. In essence they are upper and lower quality limits for the input and output of the capillary device. By relaxing these conditions slightly, the modeled pump was made more robust without affecting the steady-state solution.

Another tool which was used to prevent evaporator deprime was the subroutine SPRIME. SPRIME, short for "stay primed", is able to sense when an evaporator deprime is imminent and makes adjustments to the pressure and quality of adjacent lumps to ensure the pump remains primed. Care had to be taken while using this subroutine because although SPRIME will keep the evaporator from depriming, it may cause the program to

47

produce inaccurate results. There were two ways to ensure that the model was still valid. First, a program option was used that printed out a message every time SPRIME changed a value. A continuous stream of messages would indicate that the solution was invalid. Finally and most important, all submodel energy balances were verified to ensure validity of the solution.

A junction was used to model the evaporator vapor exhaust. With the assumption that the vapor line has already been cleared of liquid, the response of the exhaust header will not have a significant effect on the steady-state solution and selection of a junction is appropriate. The junction temperature was set at the saturation temperature, and the initial quality set to 1.0 (i.e., no liquid in vapor grooves during normal operation). If a transient response of the startup were modeled, a tank might be a better choice because state properties within a tank cannot change instantly like they can in a junction. A tank will tend to smooth the transient system response and will help keep the evaporator primed.

STUBES were used to model the liquid and vapor transport lines. A tank was also created to account for the volume of each section. The vapor side tubes reflected their 0.01021 meter (0.4 inch) inner diameter and the 4.647 meter (15.33 foot) length between the evaporator exhaust header and the condenser inlet. Due to the length and small conductive area of these pipes, axial conduction was orders of magnitude smaller than heat transfer due to fluid flow and was neglected.
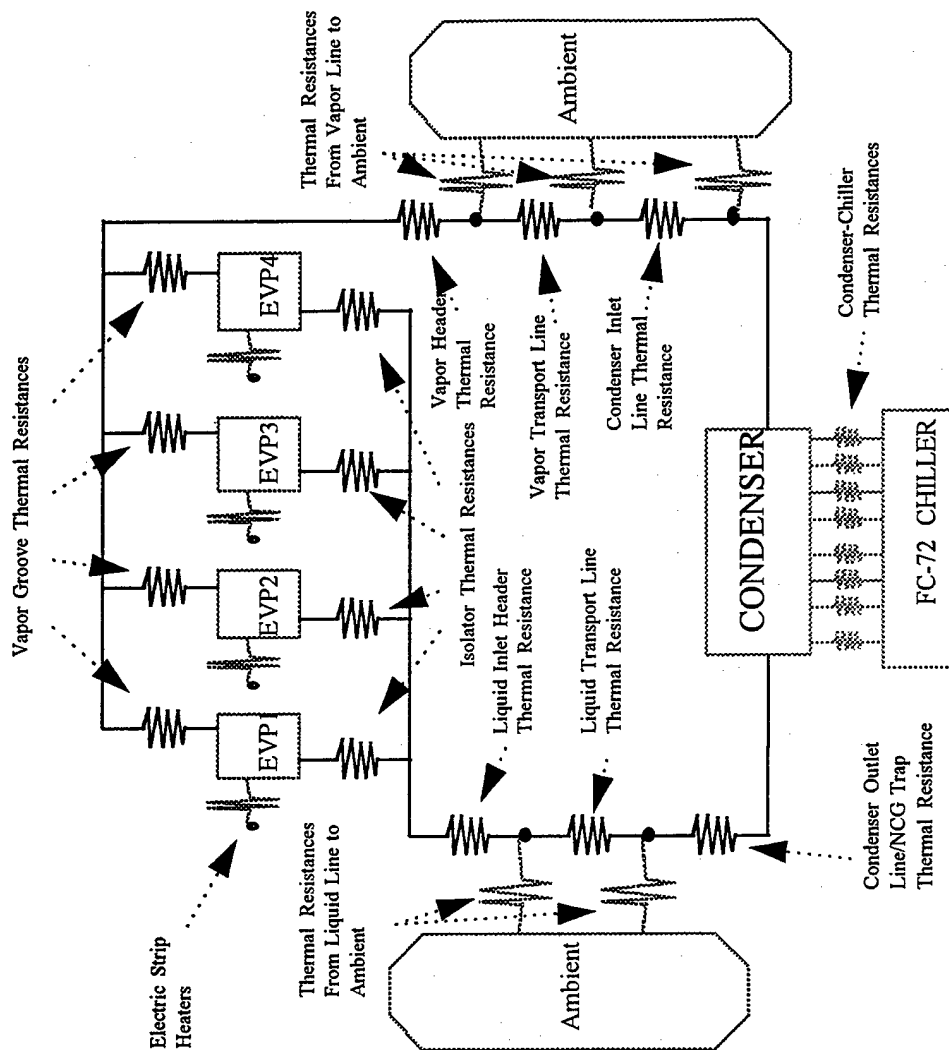
Figure 4.2. Thermal Resistance Network for the CPL Model.

49

The condenser portion of the steady-state model was the most difficult to design. The condenser for the Phillips Laboratory capillary pumped loop is different from most in that there is not a single path for fluid flow. Each condenser section contains eight parallel condenser tubes connected to inlet and outlet manifolds. The flow rates in each tube, as well as the location where condensation occurs is not as easily delineated as in single path condensers.

The eight parallel lines in the condenser were modeled as eight mini-condensers using the built-in HX macro. The eight parallel tubes were thermally connected via ties to the cold plate submodel. Although FLUINT allows for path duplication which might have simplified modeling somewhat, these factors were not used. Duplication factors assume that the flow is equally distributed between all tubes. As actual experimentation has previously shown, that is not the case. Experiments show that a majority of the vapor travels through the first three tubes, with considerably less vapor flow making it all the way down the manifold to the last several tubes. In an attempt to model this phenomenon, the eight "mini" condensers were modeled so that they were completely independent of each other, allowing for different flow rates in each condenser leg. To conform with the current test setup, only one of the condensers was modeled.

The HX macro used to model the mini-condensers was designed to model heat exchangers. Ten discrete points (junctions) were used to model each of the eight condenser legs. This number was chosen to allow for more accurate determination of where condensation actually takes place within each leg. By observing the lump quality during program output, the location of condensation may be estimated to within 10% of

the overall condenser length. Finer precision could be achieved by adding more lumps to each of the mini condensers, but would also increase simulation run time. The condenser junctions were connected by STUBE connectors, with the end connectors each 0.0912 meters (3.59 inches) long and the four interior connectors each 0.1825 meters (7.18 inches) in length. The segment lengths add up to the total condenser length of 0.733 meters (28.85 inches) per leg. They are less sensitive to flow reversals, and help with solution stability. Each STUBE reflected the 1/8 inch (0.00318 m) inner diameter of the Swales and Associates design. [Refs. 9, 16]

Thermal ties were used to connect the junctions for each of the parallel condensers to separate nodes representing the tube walls in the CLDPLT submodel. As mentioned before, ties are similar to conductors and are used to link thermal and fluid submodels. Each tie has a UA coefficient associated with it. The tie parameters may be calculated by the program itself using one of several correlation methods built into the code, or the user may define their own equation or subroutine to perform the calculations. The program calculates the heat transfer coefficient by assuming that for the time step in question, the lump represents the bulk fluid properties and the node represents the average wall temperature. Since the step size is usually small, these assumptions are very accurate for most simulations. The steady-state model incorporated HTNC ties which were recommended for two-phase flow. Although using these ties shortens the maximum time step allowed and therefore increases program run time, the ties are capable of handling the large property variations that accompany phase changes and help maintain stability during solution. [Ref. 16]

51

The initial layout of the steady-state model did not contain the noncondensible gas trap at the outlet of the condenser. The effects of noncondensible gases are not yet fully understood, and modeling them in a one-dimensional SINDA/FLUINT model would be extremely difficult. However, after reviewing system performance data, it was noted that the gas trap did play an important part in the overall system pressure drop and needed to be modeled if for that reason alone. A CAPIL device was used to model the noncondensible gas (NCG) trap, using the effective capillary radius and wick permeability provided by Swales and Associates, Inc. [Ref. 16]

The condenser inlet header was modeled as a junction. The inlet header was initially set at the saturation temperature and pressure with a quality of 1.0. The outlet header also was modeled as a junction, however some additional components were added to it to create the NCG trap. A short STUBE was connected from this junction to a tank which represented the inlet line to the NCG trap. This was done to provide stability to the CAPIL connector which connects this STUBE to a similar one representing the liquid transport line. The tank volume was input as the sum of the volume of the condenser liquid header and the NCG trap. Tank temperature was set to the subcooled temperature of 16 C and a quality of zero. These inlet and outlet headers were connected via STUBES to the eight mini-condensers to completely model the condenser section. The volume of the inlet header was accounted for in the vapor inlet line tank.

For each STUBE connector mentioned above, loss factors due to pipe bends, elbows, valves, and tees had to be examined and incorporated into the pressure loss calculations through each section. Loss data for valves was obtained directly from the

manufacturer. Table 4.1 lists the K-factor losses for each applicable STUBE in the CPL2 fluid model. Figure 4.3 shows a diagram of the CPL2 fluid submodel.

The K factors are basically velocity head factors which increase the normal flow pressure loss through each line. [Ref. 18].

$$K = \frac{\Delta P}{\frac{1}{2}\rho V^2}$$

STUBE Number	Flow into tee branch (1.9 each)	Flow out of tee branch (1.2 each)	90 degree elbow (0.74 each)	180 degree elbow (1.2 each)	Valves (0.36 each)	Total K factor
05	0	0	2	0	0	2.48*
25	2	0	10	3	7	18.36
65	0	1	2	0	1	3.14
95	1	0	4	1	2	8.56
Cond. Tubes (Inlet)	1	0	0	0	0	1.90
Cond. Tubes (Outlet)	0	1	0	0	0	1.20

* K factors in parenthesis.

Table 4.1. Pipe Flow K Factors for CPL2 Fluid Submodel.

The steady-state model contains three thermal submodels, one representing the evaporator section, one representing the condenser, and one representing the liquid and vapor transport lines. The EVP submodel is made up of six diffusion nodes with their associated conductors representing the path of heat flow from the heater strips to the evaporator wall. All conductors are of the linear type. Radiation to the environment was not included in this thermal submodel because the surfaces of the evaporator section are covered with insulation, and the differences between ambient and insulation temperature are small, making heat transfer due to radiation negligible. The heater node is an

arithmetic node to provide immediate response to heat input. The thermal capacitance of each diffusion node was left at the default value since all nodes are treated as arithmetic during the FASTIC solution method [Ref. 16]. The resistance along the heat transfer path was dominated by the contact resistance at the junction where plates and/or brackets were mounted to each other. The contact resistance was calculated using a correlation for graphite foil in the near-bolt region of the interface. Although graphite foil was used in an attempt to thermally connect surfaces, its resistance was in some cases two orders of magnitude greater than the resistance through the highly conductive aluminum. Figure 4.4 shows a diagram of the EVP thermal submodel. [Ref. 2]

The CLDPLT thermal submodel consisted of eight nodes representing the ammonia side tubing and eight nodes representing the condenser plate. The condenser itself was modeled as a sink. This was done to simplify the model, and is an accurate assumption considering the total heat input for the one-evaporator model and the cooling capability of the condenser. The temperature of the sink could be modified easily to conform to different radiator temperatures. The ammonia side tubing nodes in the CLDPLT model were attached to the condenser plate nodes via linear conductors representing the sum of the conductances through the tube wall, tube mounting bracket, graphite foil interface, and ½ thickness of the plate. The conductors between the plate and the sink were identical except for an additional term dealing with the convective conductance from the coolant flow in the condenser side tubing.

The first step in calculating this additional forced convection conductance term was to determine the type of flow through the condenser piping. The Reynolds Number

(Re), was used to make this determination.

$$Re = \frac{V*D}{\nu}$$

where V is the flow velocity, D is the interior pipe diameter, and ν is the kinematic viscosity of FC-72.

The flow rate of FC-72 through the condenser piping is regulated at 4 gpm, which equates to a Reynolds number of 3.96×10^4. This is well above the threshold for laminar internal pipe flow (~2300), and past the transition region into turbulent flow [Ref. 19]. The Dittus-Boelter equation was used as the correlation for turbulent flow to determine the convective heat transfer coefficient. Figure 4.5 shows a diagram of the CLDPLT thermal submodel.

$$Nu_D = 0.023 * Re_D^{4/5} Pr^{0.3}$$

To completely define the capillary pumped loop at Phillips Laboratory, another thermal submodel was needed. Due to the long lengths of liquid and vapor transport lines, a portion of which have no insulation, there is heat transfer between the lines and the environment. Neglecting this heat transfer causes only a slight error in flow rates and pressure drops, but causes discrepancies in vapor and liquid line temperatures.

The vapor-liquid line thermal submodel (VLL) was included to account for heat transfer to and from the environment. It consists of nodes representing significant segments of each line. For the vapor side, there are nodes to represent the vapor exhaust header, the vapor transport line, and the condenser inlet line. For the liquid side, there are nodes representing the NCG trap outlet line, and the liquid transport line. Each node is connected via a linear conductor to the environment. The nodes in the VLL submodel are

also thermally tied to a corresponding fluid lump to account for heat transfer to and from the ammonia flowing in the system. HTN ties were used because the flow in each section is single phase.
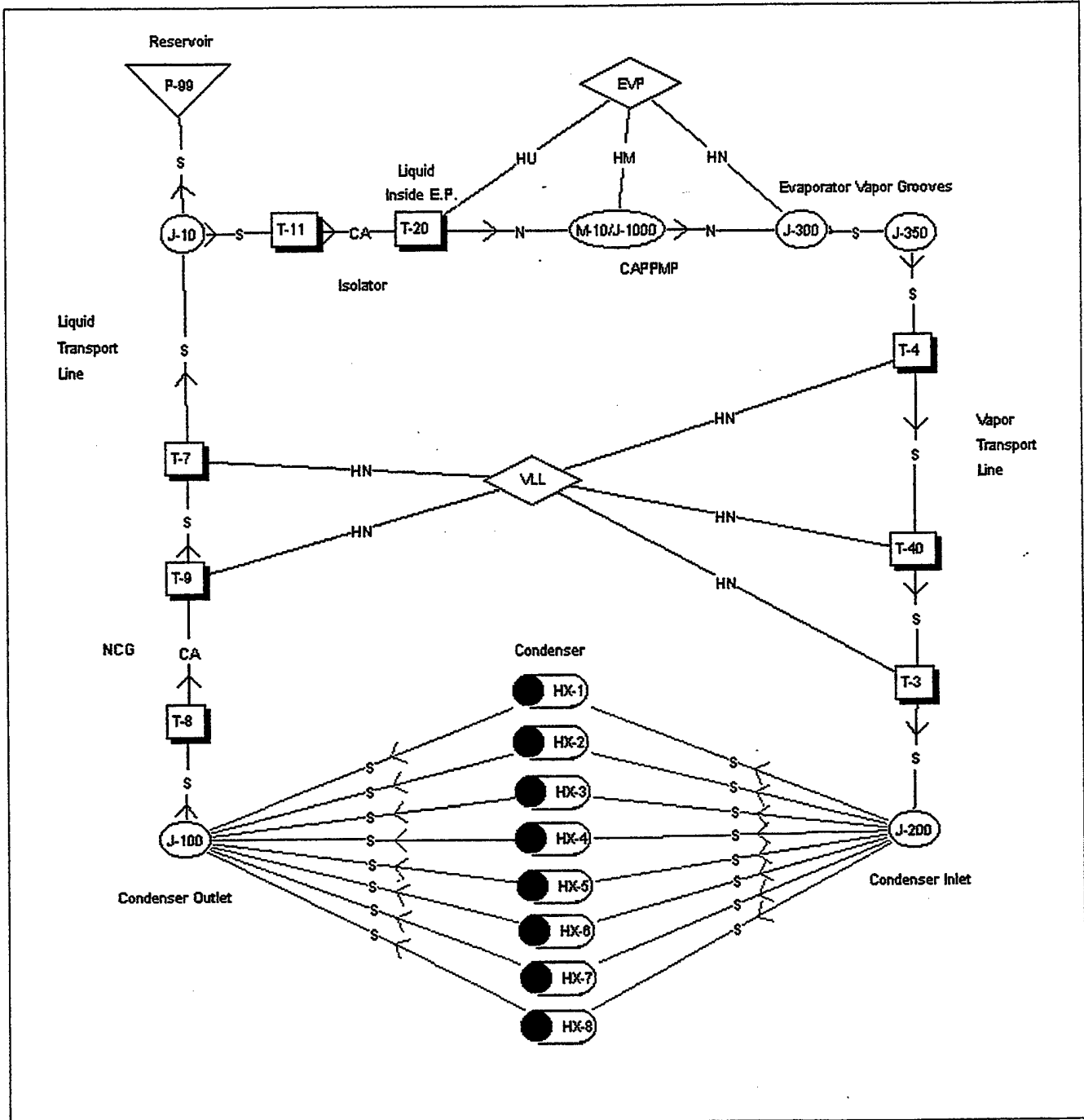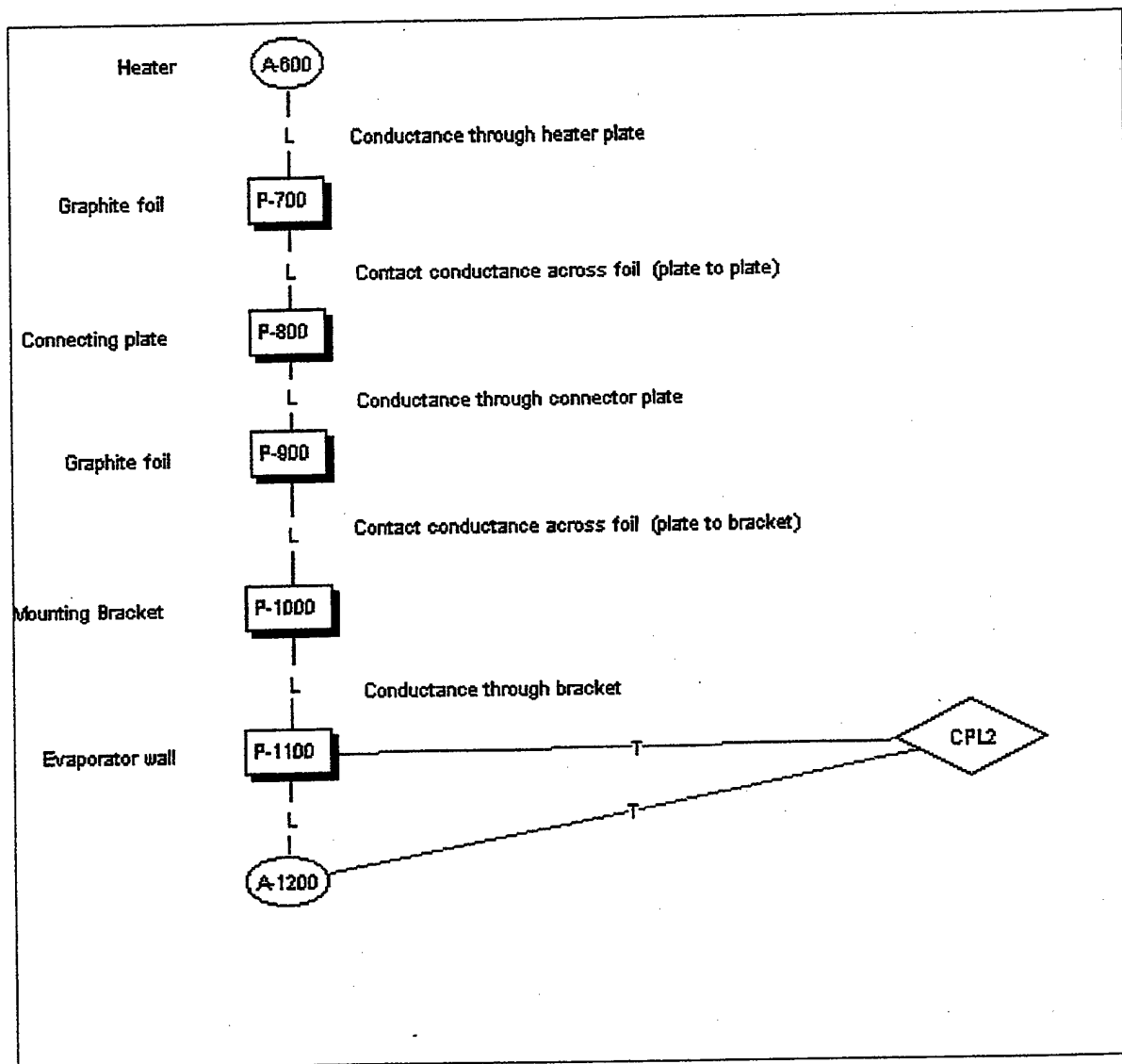

Figure 4.3. CPL2 Fluid Submodel Diagram.

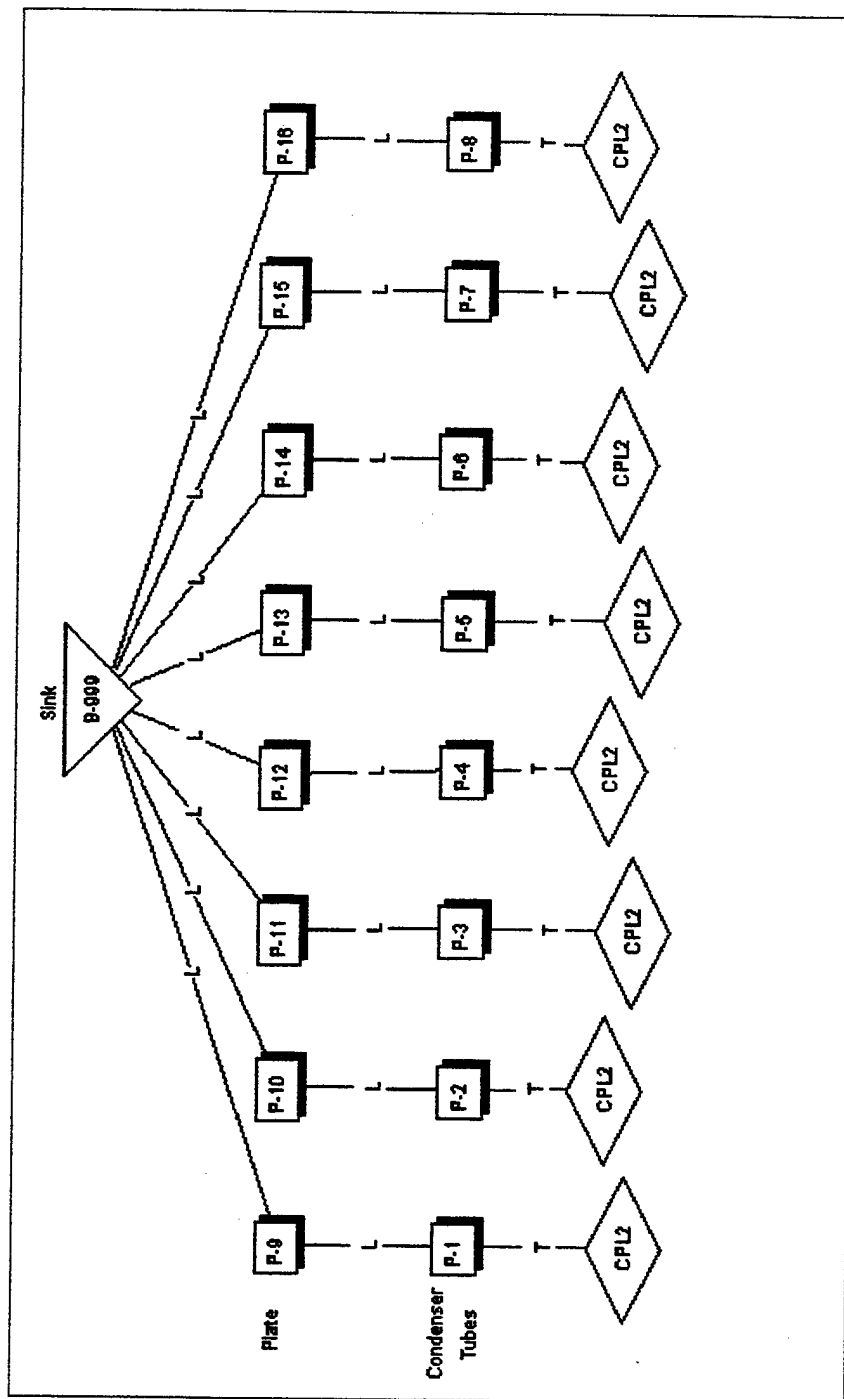**Figure 4.4. EVP Thermal Submodel.**

Figure 4.5. CLDPLT Thermal Submodel.

The tube walls experience heat transfer via four methods: axial conduction along the tubing, natural convection with the surrounding air in the laboratory, forced convection from fluid within the tube to the tube wall, and radiation to and from the surroundings. To simplify the model, axial conduction and radiation were neglected. The conductances for both of these heat transfer paths were small in comparison to natural convection and internal convection. The axial conductance of the nodes closest to the reservoir were calculated to be less than 0.001% of that for natural convection, and the radiative conductance was less than 0.01% of that for natural convection.

The conductance input for each node consisted of two terms. First, the radial conduction through the tube wall and insulation, if applicable, was calculated. The equation used is shown below.

$$C = \frac{2 * \pi * k * L}{\ln(r_o/r_i)}$$

The next conductance which had to be calculated was the conductance due to natural convection. To determine the natural convection equation to be used, the process itself had to be examined. The surface of the tubing will either cool or warm a layer of surrounding air, making it gravitationally unstable with the rest of the air in the room. There will be a tendency for the cooler, more dense air to flow downward, and the warmer, lighter air to rise. The fluid motion caused by the density differences causes convective heat transfer between the tube and this small layer of surrounding air. To calculate the conductance due to natural convection, the Rayleigh number had to be determined.

$$Ra = \frac{g*\beta*(T_w - T_\infty)*L_c{}^3}{\nu\alpha}$$

In this equation, g is the gravitational acceleration, β is the expansion coefficient, L_c is the characteristic length, α is the thermal diffusivity, and ν is the kinematic viscosity. In the above expression, both β, ν, and α are properties of the surrounding fluid at the ambient temperature. With the assumption that air behaves like an ideal gas, β is simply 1/T. The L_c term is simply the diameter for natural convection over a horizontal cylinder, and is equal to the surface area divided by the perimeter for the case of natural convection over a flat plate. For the conductors tied to the bare tubing of the NCG trap outlet line, the evaporator exhaust line, and the condenser inlet line, the horizontal cylinder correlation was used. For the insulated transport sections, the following correlation for the average Nusselt number based on free convection from the upper surface of a heated plate was used. [Ref. 19]

$$Nu_D = 0.54*Ra_L{}^{0.25}$$

As a first approximation, a temperature difference was assumed, the Rayleigh number calculated, and test runs using 100 and 200 watts were completed. The average temperature difference along the liquid line was observed for both of these test runs. These temperature differences were averaged and then substituted into the Rayleigh number calculations to come up with an "average" Rayleigh number. Figure 4.6 shows a diagram of the VLL thermal submodel.

Once the model was built, the next step was tailoring the solution procedure using the model control panels and Fortran-style logic. The most important of these logic

control panels is the Operations Data block. In this block Fortran-style code must be input to command the processor to build the code based on SINAPS inputs. Each submodel must be correctly built and connected to create the complete capillary pumped loop model. The solution method must be selected in this field. The FASTIC solution procedure was selected. The ability of this procedure to smooth initial conditions helps stabilize the solution, and is the recommended solution procedure when large fluid submodels are present. The start and end times, step time, and maximum number of iterations per time step must also be input here.

The other logic blocks deal mostly with tailoring the output of each submodel for use in post-processing. By instructing the program to output only desired parameters at desired intervals, the run time and storage requirements may be reduced.

C.   TRANSIENT MODEL

Modifications were made to the existing steady-state model to create the model used in transient solutions. Thermal capacitance was calculated and added for each of the diffusion nodes in the EVP, VLL, and CLDPLT thermal submodels. A starter pump was added and connected directly to the reservoir to simulate the bayonet. Although the starter pump was turned off at the start of each run, it was included in the transient model to accurately represent the piping between the pump and the reservoir. The tube connecting the reservoir to the rest of the system could not be disregarded as in the steady-state model. As conditions change, the reservoir may have to accommodate slight changes in system inventory until equilibrium is reached.

61
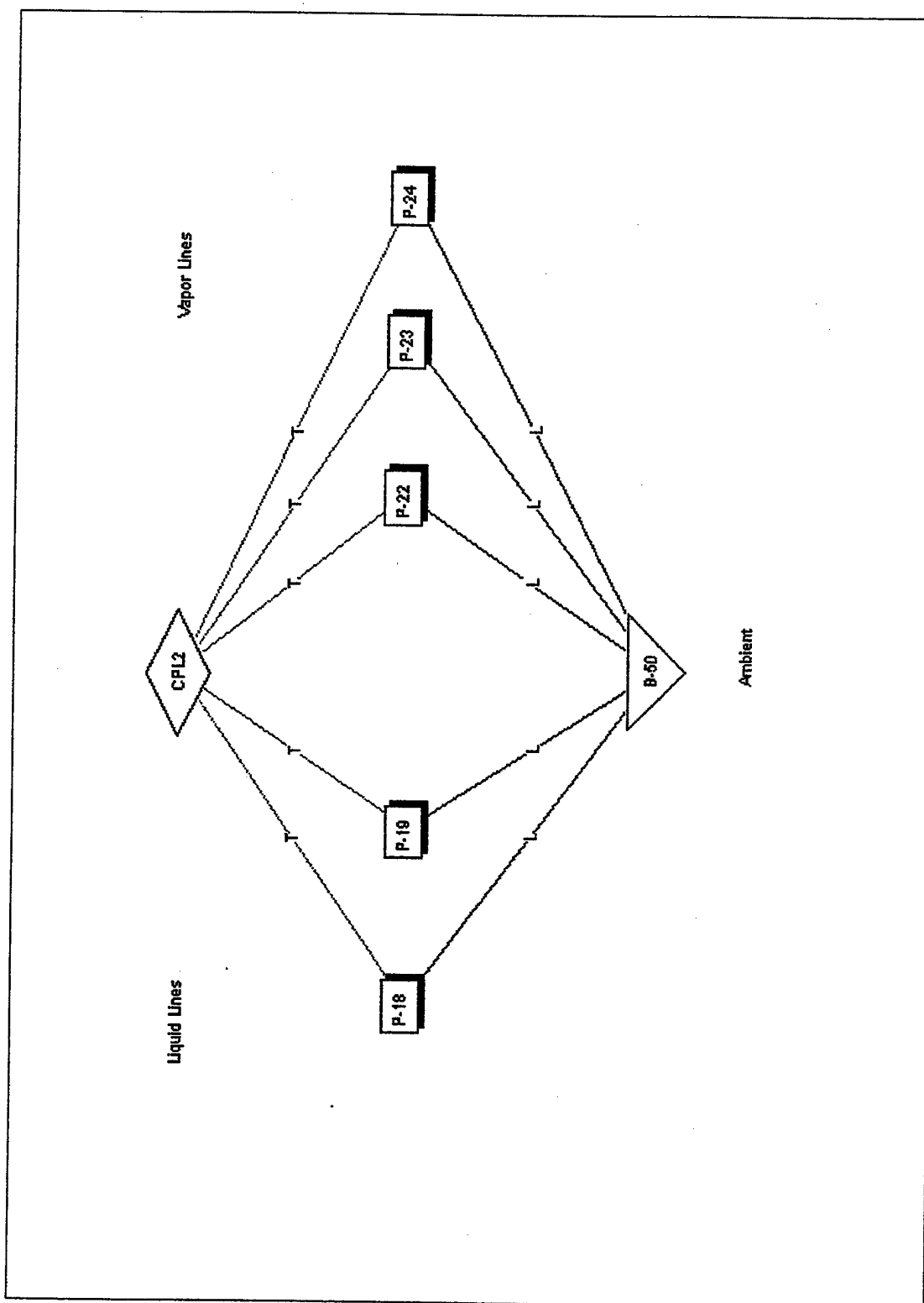
Figure 4.6. VLL Thermal Submodel.

The changes in solution procedure were the major alterations implemented for the transient modeling. A forward differencing technique (FWDBCK) was selected as the solution method for the transient model. Fortran-style logic was again used to change input parameters during the solution so system response could be observed. The solution time had to be modified to provide enough time for the system to steady out after changes so values could be compared to those produced during steady-state modeling. Figure 4.7 shows the transient CPL2 fluid submodel.

Figure 4.7. Transient CPL2 Fluid Submodel.

V.   RESULTS

A.   STEADY-STATE

To verify the accuracy of the steady-state model, the program was run with different combinations of evaporator power input and condenser set point temperature. The data produced during each run was compared to actual test data from experiments conducted at Phillips Laboratory. System temperatures and pressures were used to compare data to experimental results. The plentiful number of thermocouples positioned throughout the test setup facilitated overall temperature comparison, however attempts to compare system pressure drops were more difficult. There are only five differential pressure transducers in the Phillips Laboratory test setup. Modeling the exact location of these transducers closely enough to produce an accurate comparison was not practical. For this reason, only the pressure *profile* was compared to actual test results. The pressure *profile* is a measurement of component pressures at a specific instant in time. To facilitate presentation, pressure data is plotted for the entire loop. The plots begin with the evaporator vapor grooves (highest pressure in the system) and continuing along the loop until reaching the component with the lowest pressure in the system, the evaporator liquid core. Pressure profiles for 100, 200, and 300 watts (condenser temperature -5 C) are provided in Figures 5.1 through 5.3.

The profiles displayed in the figures mirror those of actual testing, with the larger pressure drops occurring across the wicked devices such as the noncondensible gas (NCG) traps and the isolator. In each case, the pressure rise across the evaporator wick is

large enough to overcome the losses through the system. As expected, increased power input to the evaporator was accompanied by larger flow rates and larger pressure drops.
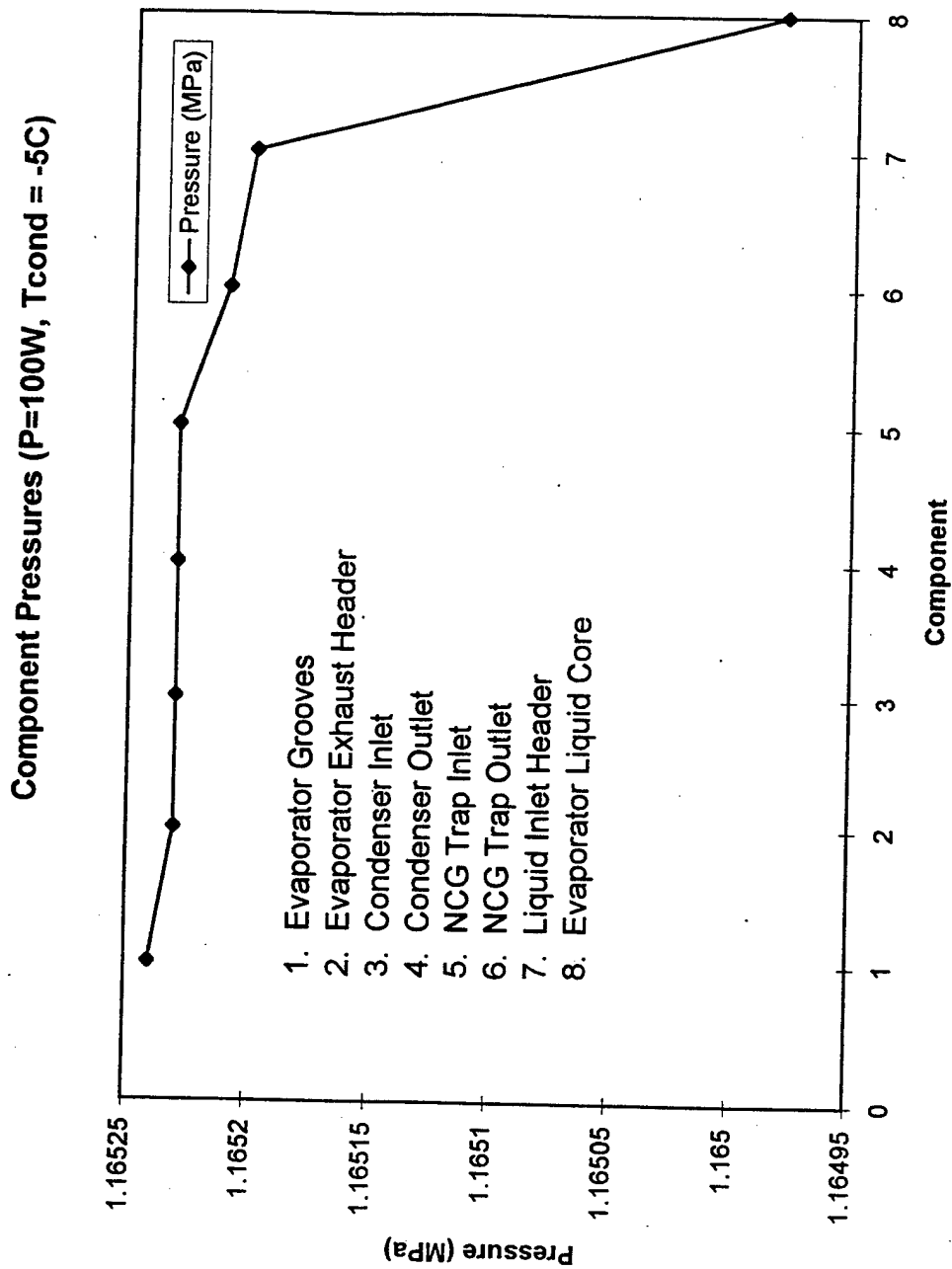
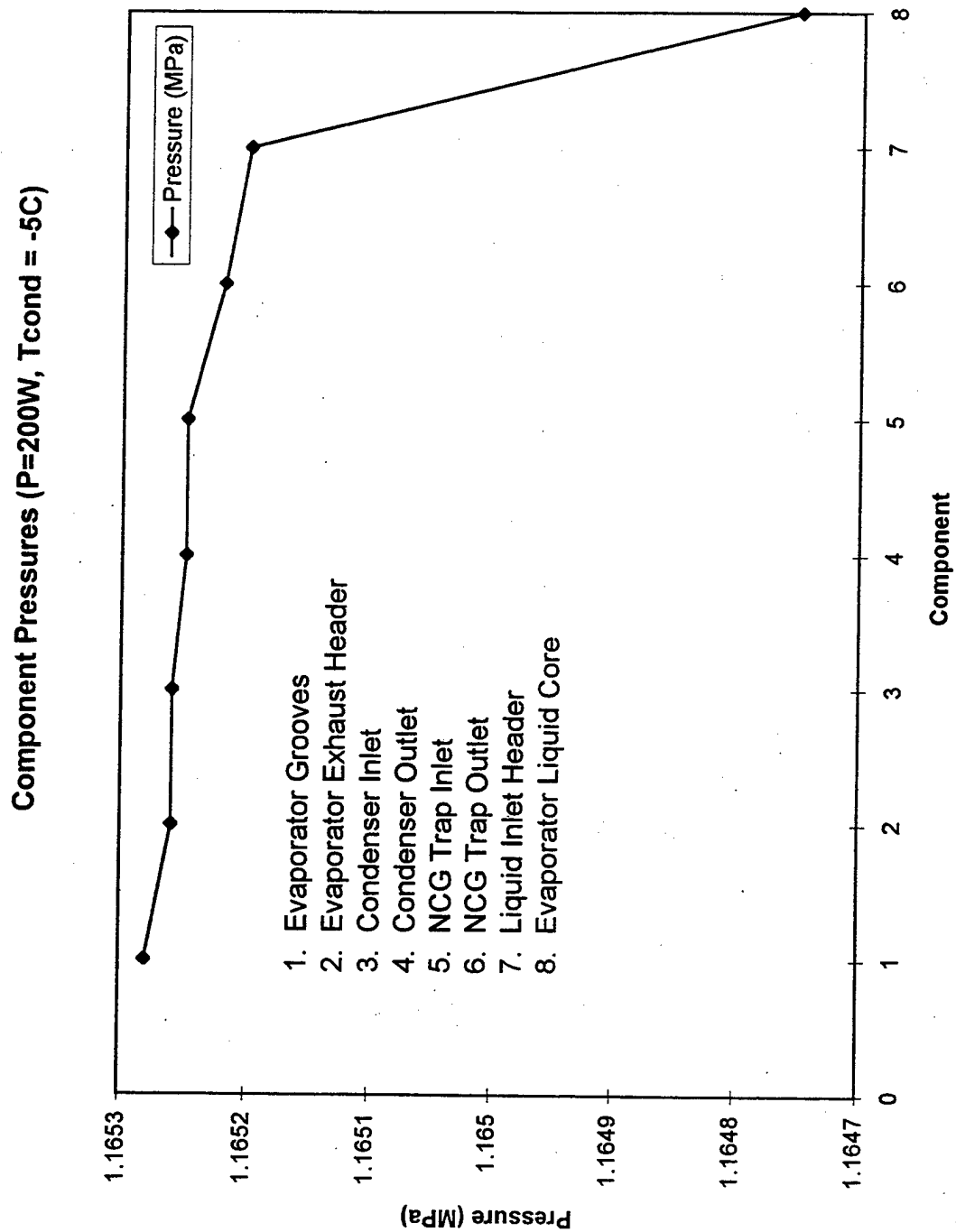Figure 5.1. CPL Pressure Profile (100 Watts, Condenser –5 C).

Figure 5.2. CPL Pressure Profile (200 Watts, Condenser –5 C).

67
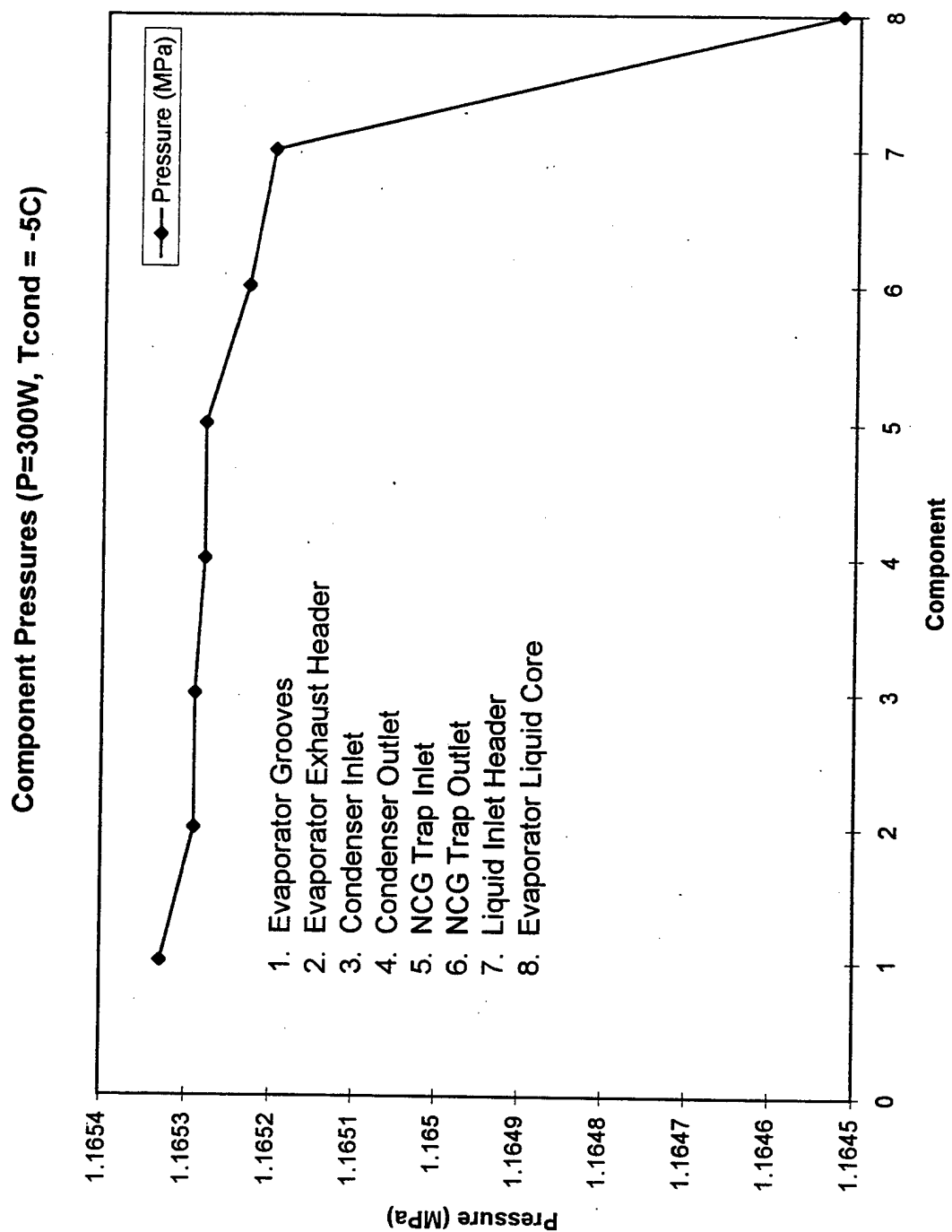
Figure 5.3. CPL Pressure Profile (300 Watts, Condenser –5 C).

The pressure profiles of the steady-state model are useful in that they show where the majority of the system pressure losses occur. As expected, pressure changes in the liquid and the vapor transport lines, as well as the condenser were small. Appendix C contains pressure profiles from the other steady-state runs. The pressure losses are driven for the most part by system flow rates, and profiles for all steady-state runs were similar since the condenser temperatures modeled (-5, 0, and 5 C) had little effect on system flow rate. In all runs the pressure losses were within the capillary limit of Evaporator Pump No. 4.

For temperature data comparison, nine different steady-state runs were completed. Each run was based on a different power input to evaporator No. 4 and/or a different condenser set point temperature. To create meaningful plots of temperature data, a complete "loop" of system temperatures was plotted for each run. The upper left of each plot shows the evaporator vapor grooves and vapor transport line. The steep slope occurs as the working fluid enters the condenser, where the plot levels off somewhat before rising again as the working fluid exits the condenser and proceeds back to the evaporator section. Figures 5.4 through 5.6 show data comparisons for the 100-Watt steady-state simulations.

The model indicates the working fluid exits the evaporator as a slightly superheated vapor which cools rapidly to saturation temperature as it travels through the uninsulated vapor header. The temperature data remains constant along the vapor transport line, where the model also predicts condensation to commence. The steep slope between points 6 and 7 reflects the rapid condensation of the working fluid, which both

69

the model and the experimental data show to occur in the first portion of the condenser. The differences at point 6 (condenser inlet) are due to differences between the model and the test setup as to thermocouple placement within the condenser. A relatively small physical distance can cause large temperature variation in this region where the phase change is taking place.
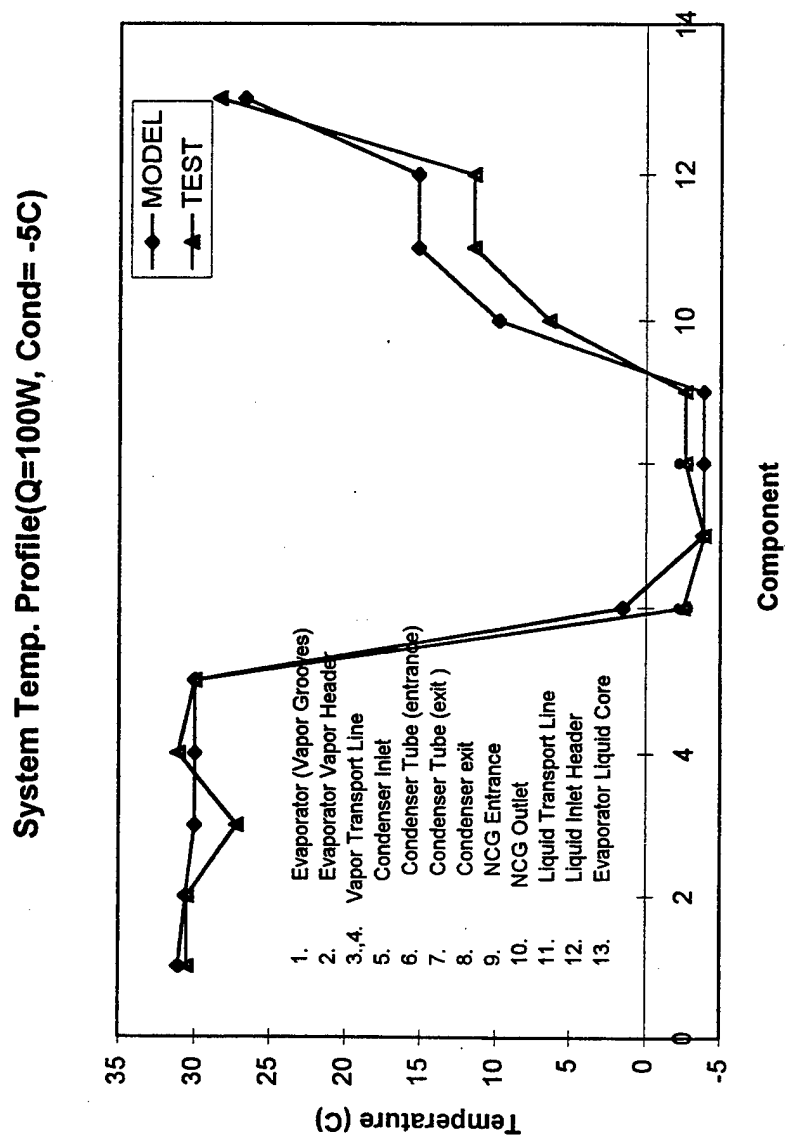
Figure 5.4. Temperature Data Comparison (100 W –5C).
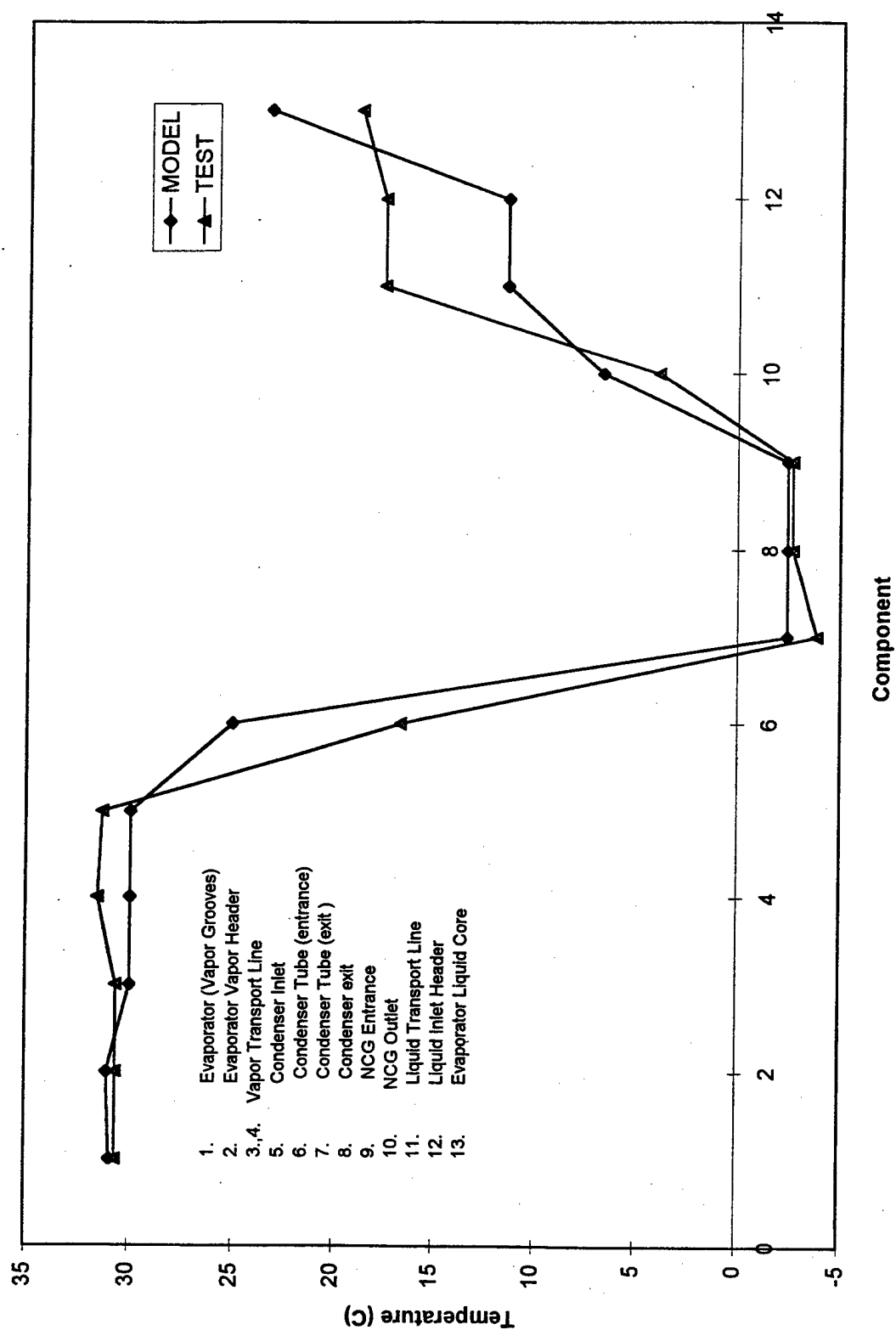
Figure 5.5. Temperature Data Comparison (200 W –5C).

System Temp. Profile (Q=300W, Cond= -5C)

1. Evaporator (Vapor Grooves)
2. Evaporator Vapor Header
3.,4. Vapor Transport Line
5. Condenser Inlet
6. Condenser Tube (entrance)
7. Condenser Tube (exit)
8. Condenser exit
9. NCG Entrance
10. NCG Outlet
11. Liquid Transport Line
12. Liquid Inlet Header
13. Evaporator Liquid Core
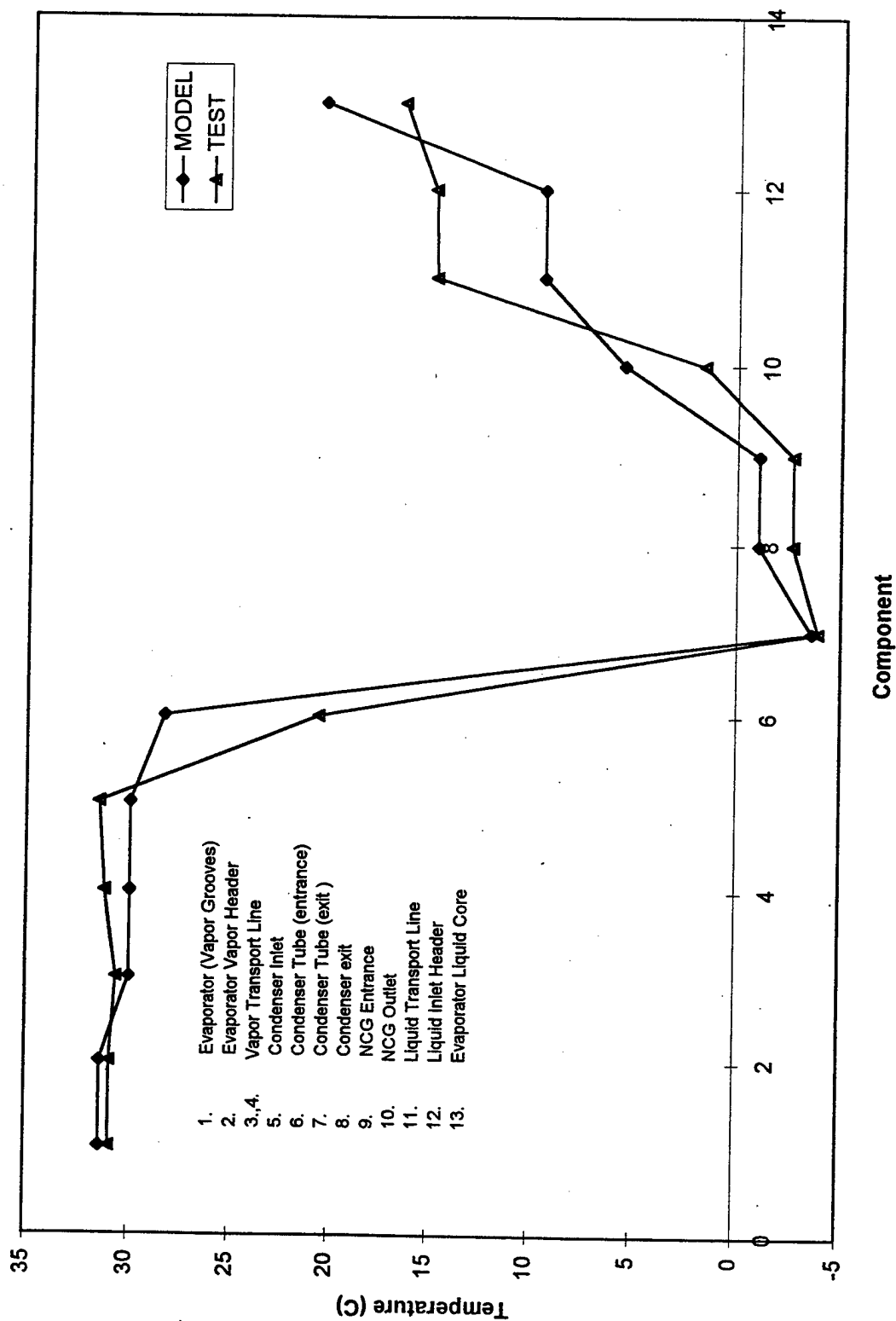
Figure 5.6. Temperature Data Comparison (300 W –5C).

72

At the exit of the condenser, both test data and the model predict a temperature rise. It is in this portion of the plots, however, that the largest discrepancies exist. The experimental data shows a marked increase in temperature occurring at the outlet of the noncondensible gas trap, where the cool liquid coming from the condenser meets the warmer liquid in the liquid transport line. The model predicts a more gradual temperature rise, with significant heating occurring in the evaporator liquid core due to back-conduction through the evaporator wick.

There are several possible causes for the differences in data for the return part of the capillary loop:

1. The model assumed a reservoir temperature of 30 C, where in experiments this temperature varied between 31 and 35 C.

2. While the model took into account the uninsulated portions of the liquid transport line, the heat transfer coefficients calculated and the ambient temperature used were possible sources of error. The model actually predicts condensation to begin along the uninsulated vapor exhaust header. Figure 5.7 shows the uninsulated portion of the vapor exhaust header.

3. The back-conduction of heat through the evaporator wick may have been overestimated in the model.

4. As mentioned earlier, thermocouple placement and accuracy also contribute to temperature differences. The model predicts the temperature of the working fluid, whereas in most cases the thermocouples are recording the tube wall temperature.

5. The SINDA/FLUINT model assumes an ideal inventory of working fluid in the

capillary pumped loop. The inventory of ammonia in the actual test setup is unknown, and may actually be less than the amount used in the model.

6. Thermophysical properties used in calculating heat transfer coefficients for conduction and convection were only accurate to $\pm$ five percent.

The overall temperature profiles bear close resemblance in all cases, validating the accuracy of the steady-state model. The addition of more nodes in the condenser and liquid transport line submodels may improve the results somewhat, but would also increase complexity and run time.

Temperature data comparisons for the 200 and 300-Watt simulations are provided in Appendix D.
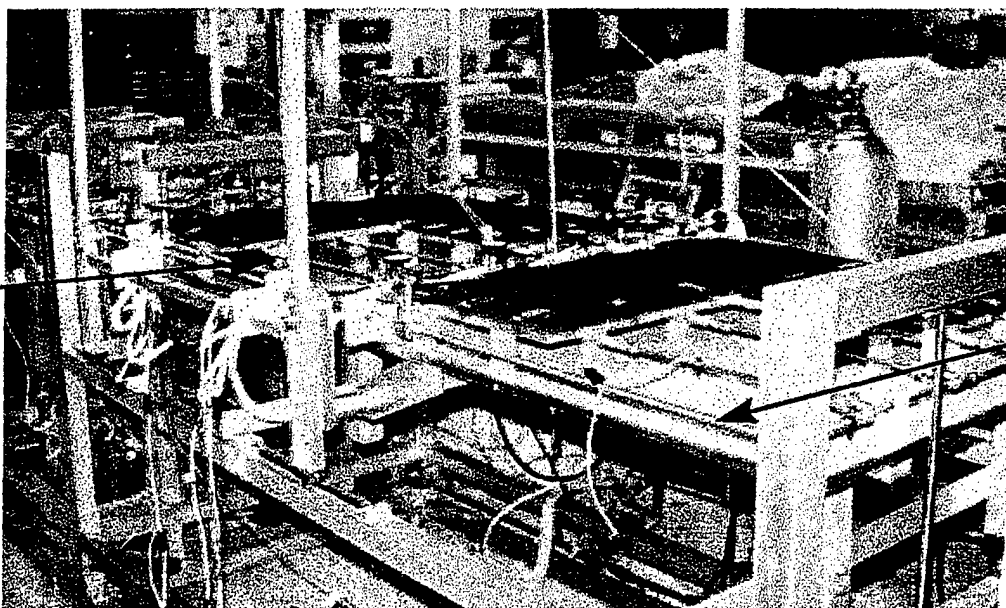
Figure 5.7. Uninsulated Portion of the Vapor Exhaust Header.

B.   TRANSIENT MODELING

The purpose of the transient modeling was to examine the system response to changes in power input and condenser set point temperature. Several scenarios were run and compared to experimental data from Phillips Laboratory. Temperature and mass flow rates were compared for each run. As shown in Figure 5.8, changes in power input to the evaporator resulted in corresponding changes in temperatures and mass flow rates within the loop, which eventually reached steady-state values. The steady-state values reached in the transient solution were within two degrees of the steady-state solution calculated earlier for the same condenser set point temperature and power input. Table 5.1 summarizes the transient runs made. For each run, plots of temperature, system mass flow rate, reservoir mass flow rate, and condenser quality were made. The results are provided graphically in Appendix E.

Run Number	Transient Event Modeled
1	Power change from 300-50 watts, Condenser temperature constant (0 °C)
2	Condenser temperature changes (5 to 0 to –5°C) Power constant 200 W
3	Power change 200-300-100 watts, Condenser temperature constant (0 °C)
4	Power change 200-100 watts, Condenser temperature constant (5 °C)
5	Power change 50-300 watts, Condenser temperature constant (15 °C)

Table 5.1. Transient Run Summary.

Of particular interest was flow into or out of the reservoir. When compared to system flow rates, the flow to or from the reservoir was negligible. Even with evaporator No. 4 running at its maximum power, condensation still took place at or near the entrance to the condenser tubing, as shown in Figure 5.9. With the condenser being so efficient at condensing the vapor, there was little change in the location of the liquid-vapor interface

within the loop. With no appreciable change in fluid inventory, the reservoir did not have

to act to maintain a balance, and therefore flow in the reservoir piping was negligible.
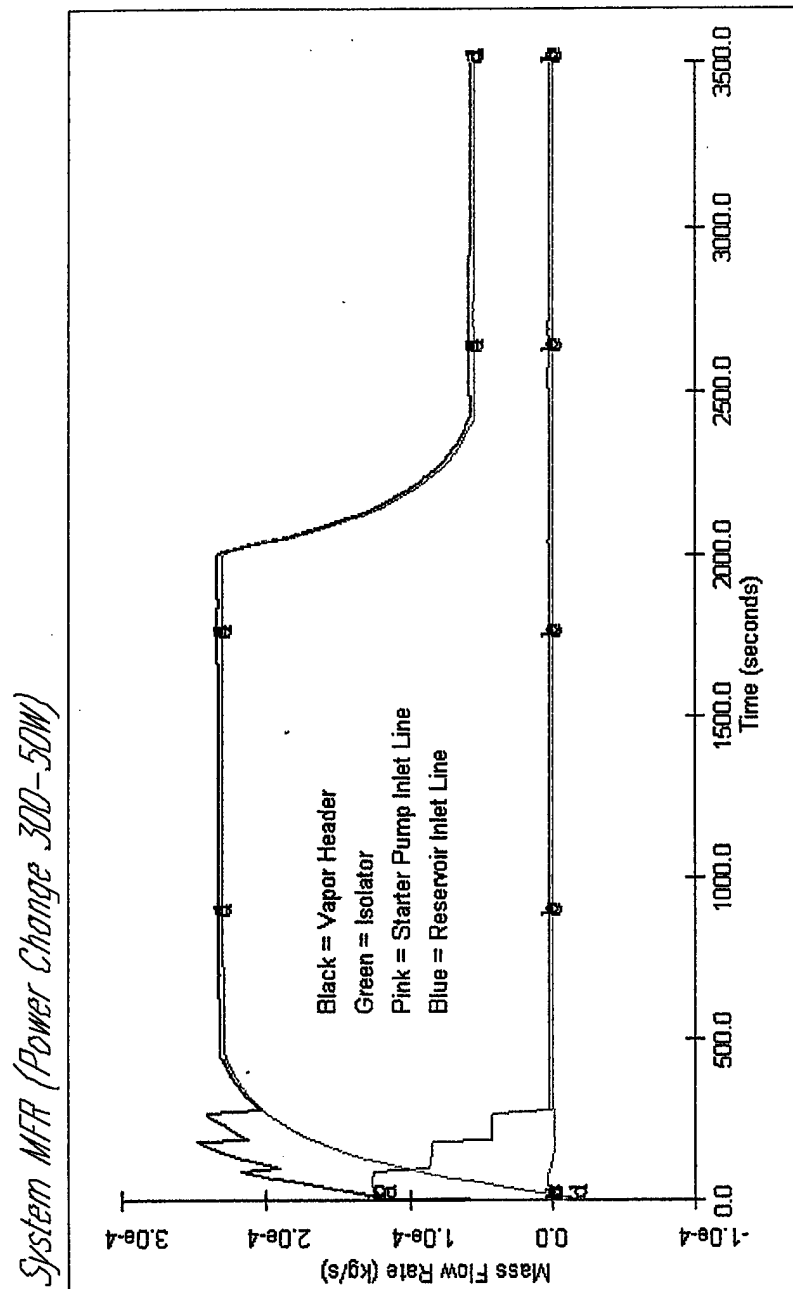
Figure 5.8. System Mass Flow Rate (Power Change from 300-50 Watts).
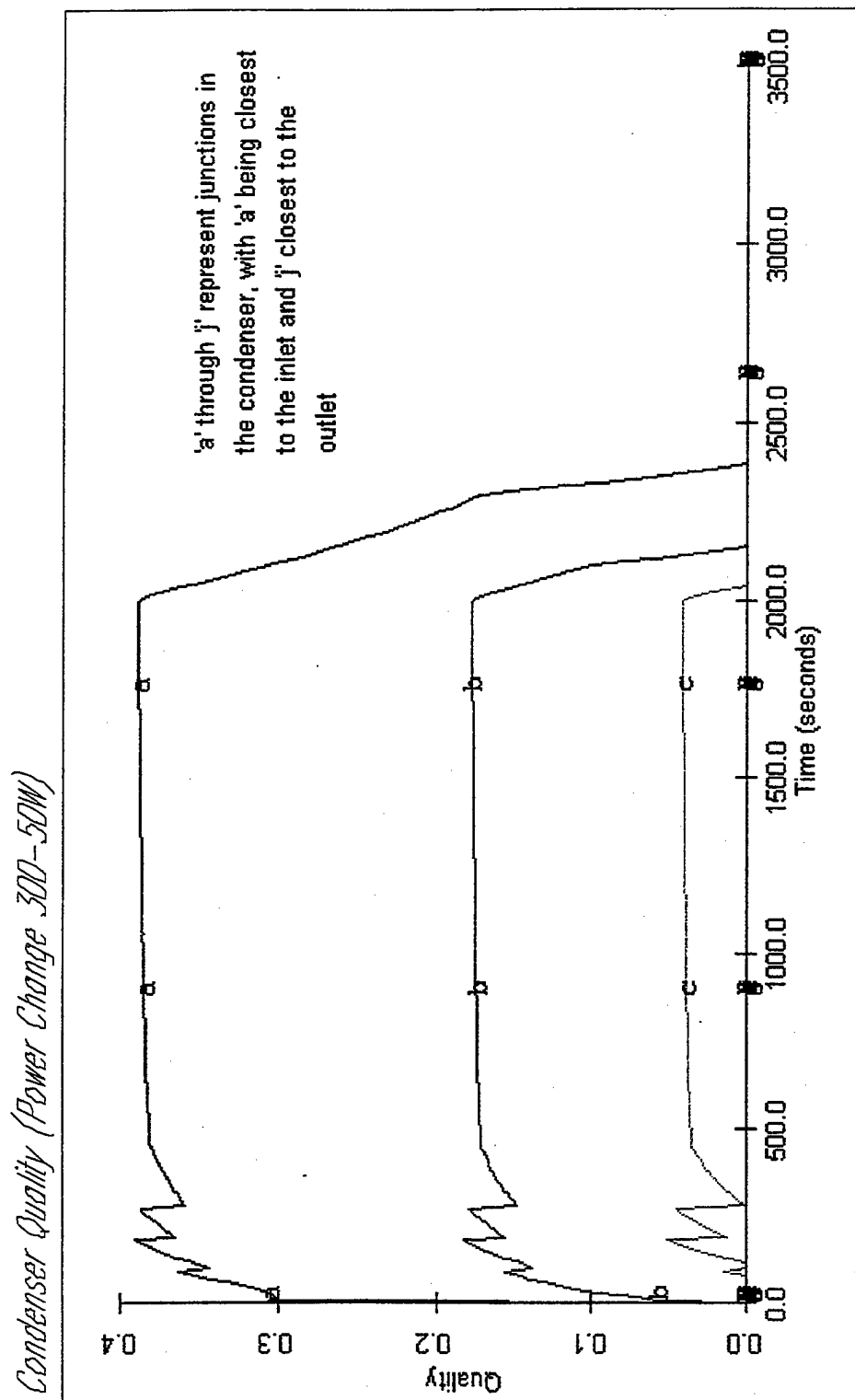
Figure 5.9. Condenser Quality (Power Change from 300-50 Watts).

77

To produce a change in flow rate to or from the reservoir, there had to be a visible shift in the liquid-vapor interface within the condenser. To model this without increasing the number of evaporators rejecting heat via the same condenser, the condenser set point temperature was increased to 15 C. A power change from 50 to 300 watts was imposed on evaporator No. 4, and the resulting reservoir mass flow rate observed. For this run, when the power was increased to 300 watts (t = 1000s), there was a corresponding spike in the reservoir flow rate (see Figure 5.10). The spike, which was an order of magnitude greater than the steady-state flow rate, lasted approximately one minute before quickly damping to zero as the system again approached equilibrium. The increase in vapor generated by the power addition caused a slug of liquid to be displaced from the condenser and eventually travel into the reservoir. The slight time delay in the spike is because the liquid must pass through the NCG trap and the starter pump header prior to reaching the reservoir inlet line.

Comparisons were made between the test data and the model for the power change of 200-300 watts during model run number three. The time required for temperatures to change and stabilize to their new values was examined. The small temperature variation in the vapor portions of the loop made comparison difficult, and therefore only the liquid portion was analyzed. For four sections of the liquid side of the loop, temperature-time data for the experiment was plotted along with model data for the same time period. The time constant for each plot was compared. Figure 5.11 displays a plot of one of these comparisons. As the plot shows, the response of the modeled NCG outlet temperature is very similar to the experimental data. The calculated time constants

for the model and the experimental data were 257 seconds and 218 seconds respectively.

Similar plots for the other sections of the liquid line are provided in Appendix F.
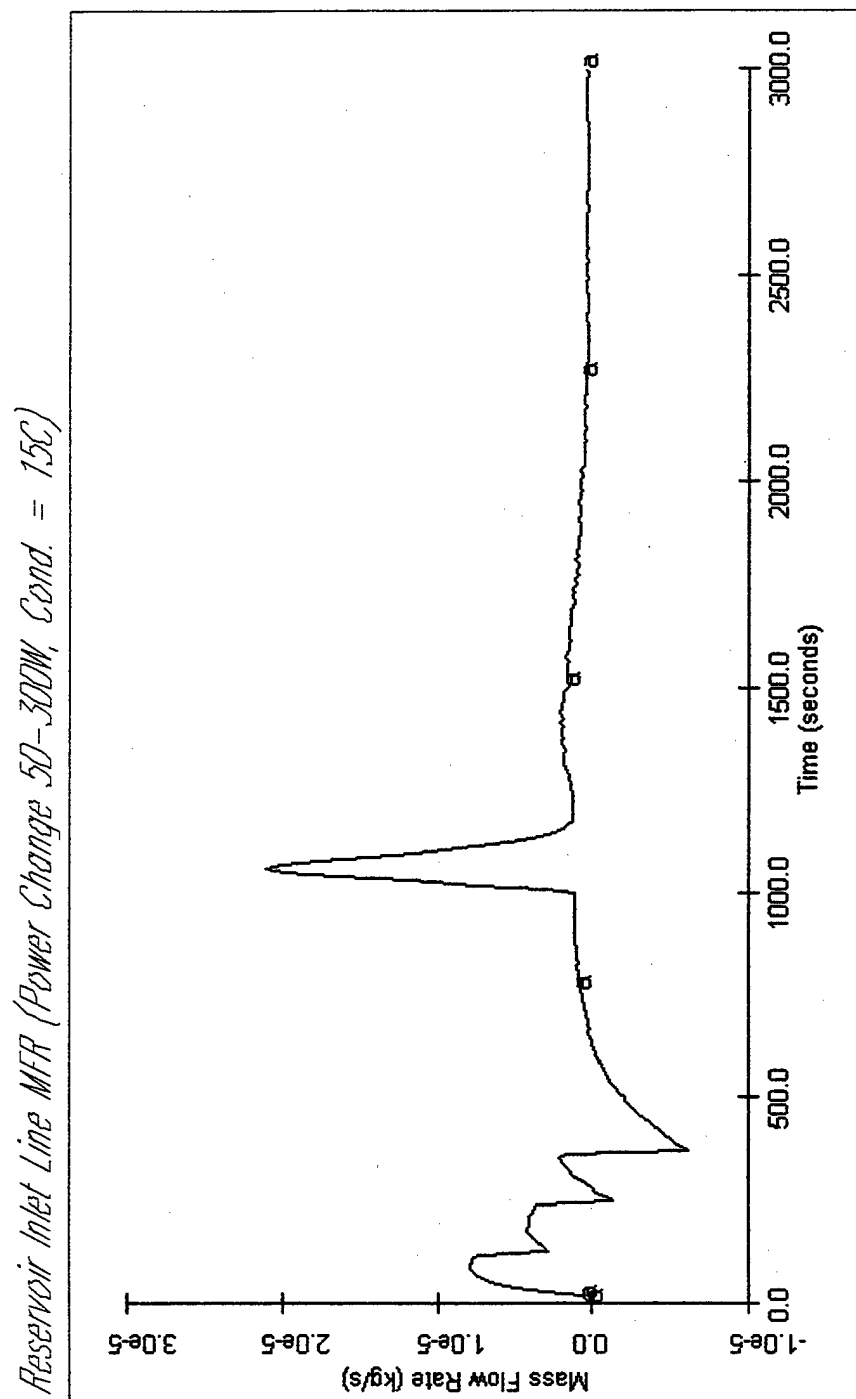
Figure 5.10. Reservoir Mass Flow Rate (Power Change 50-300W, Cond. = 15 C).

NCG Outlet Line Temperature Profile
(Power Change 200-300W)
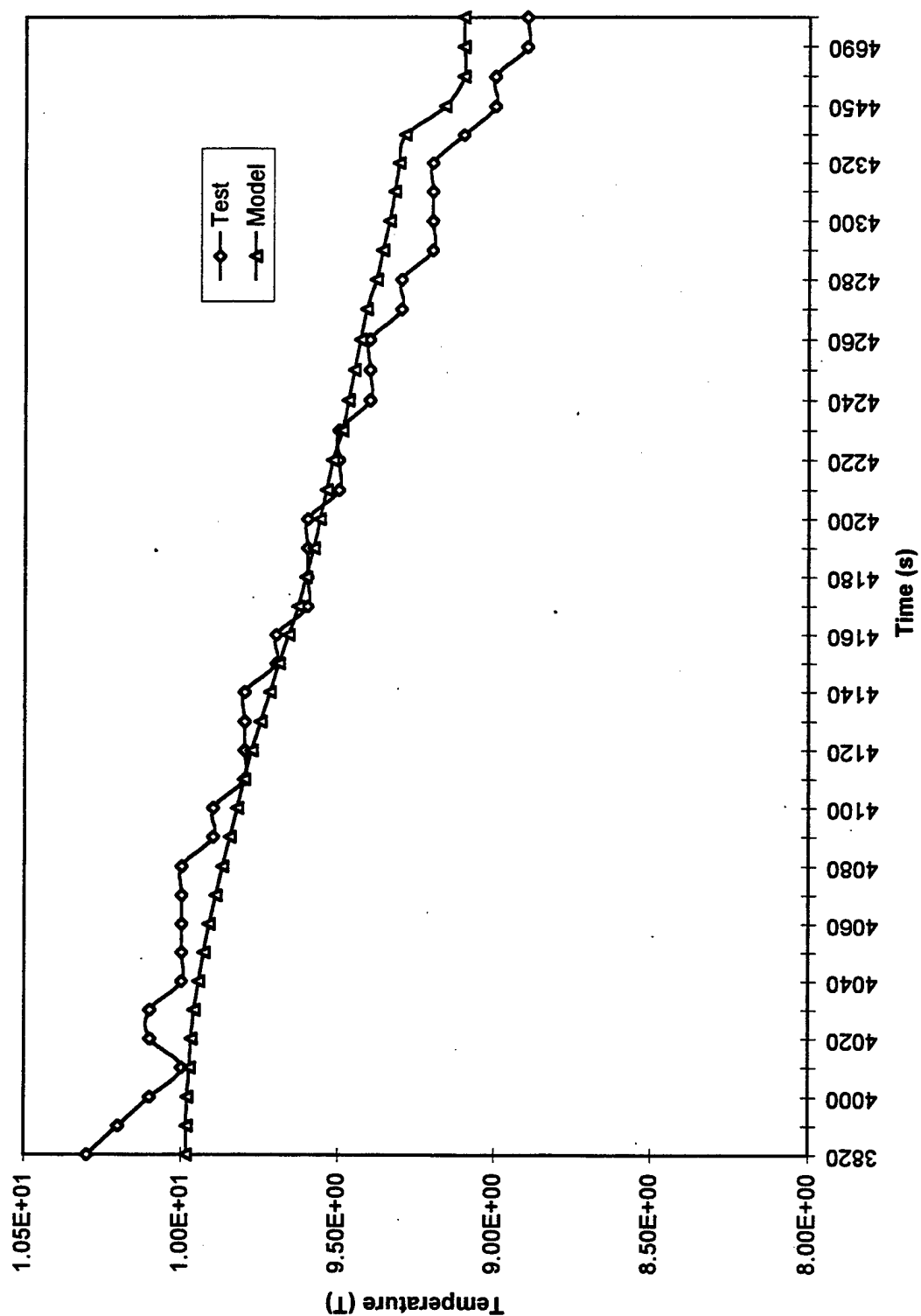
Figure 5.11. Temperature-Time Response Data Comparison.

80

VI. RECOMMENDATIONS

The models constructed in this research accurately simulate both steady-state and transient performance of the Phillips Laboratory capillary pumped loop, and are a solid foundation for continued modeling research. Continued computer-oriented CPL research should be focused on two principle areas. First, several improvements to the existing model should be investigated. Second, the addition of the other five evaporators, isolators, and heaters should be made to produce a complete model of the entire CPL.

The following are some recommendations for improving the model.

1. The model may be simplified wherever possible to shorten computation time and make the model easier to maintain. Specifically, the EVP submodel may be simplified by combining nodes and conductances to effectively shorten the path between the heater strip and the evaporator itself. Calculator registers and default parameters may also be incorporated to simplify maintenance and compilation time.

2. The VLL submodel conductances and the back-conduction effects through the wick may be modified to produce a more effective model of liquid line temperatures. The conductances for natural convection may be modified or possibly combined with radiation effects to better simulate heat transfer to and from the transport lines. The back-conduction in the model overestimated the coupling between the saturation node and the liquid within the evaporator core. The calculations were based on the assumption that the wick was 50% "wet", and this assumption may be altered to produce more accurate results. In addition, the test setup itself may be altered to include insulation along the

81

entire vapor and liquid transport lines. This would simplify the models and would help delay the onset of condensation until the vapor reaches the condenser.

3. The condenser section of the CPL2 fluid submodel does not take into account the manifold effects of the liquid inlet header, and therefore fails to show the flow patterns of the actual condenser tubes. Future study should attempt to define the pressure variation along the condenser inlet header to more accurately distribute flow through the individual condenser tubes.

4. The uncertainty as to the CPL ammonia inventory, although not a major factor in the one evaporator model, may produce more significant discrepancies when the full system is modeled. Emptying and recharging the Phillips Laboratory CPL would validate model assumptions and help with solution accuracy.

It is important that additions to the existing model be made slowly. As stated earlier, even small modifications to the fluid submodel can drastically alter results and possibly cause instabilities. Each change should be validated by comparison to existing test data. In addition to adding the full complement of evaporators, adverse elevation effects and modifications to the liquid and vapor transport lengths should be made to increase the performance database.

In conclusion, SINDA/FLUINT computer modeling is an important part of the overall evaluation of the Phillips Laboratory capillary pumped loop test bed, and could possibly pay large dividends in the latter phases of the test program. By using a computer to simulate the effects of adding new hardware or modifying the system configuration, potential problems may be discovered and dealt with prior to conducting actual

experimentation of the system. The savings in both cost and man-hours resulting from computer modeling could be significant.

APPENDIX A. SINDA/FLUINT NOMENCLATURE

This appendix provides a list of program-specific terms and abbreviations used in the description of model development.

AF -	Flow area
CAPIL -	Capillary device model
CAPPMP -	Capillary pump macro
CLDPLT -	Cold plate thermal submodel
CFC -	Flow conductance factor
COMP -	Tank compliance
CPL2 -	CPL fluid submodel
DH -	Hydraulic diameter
DUPI -	Duplication factor
EVP -	Evaporator thermal submodel
FASTIC -	Fast initial conditions steady-state solution routine
FLUINT -	Fluid integrator
FORWARD -	Forward differencing solution routine
FR -	Flow rate
FWDBCK -	Forward-backward differencing solution routine
G -	Conductance
HTNC -	Centered-lump convection heat transfer tie
HTN -	Convection heat transfer tie
HX -	Heat exchanger macro
Hl -	Head loss
QDOT -	Heat transfer rate (W)
RC -	Effective 2-D capillary radius
SINAPS -	SINDA Application Programming System
SINDA -	Systems Improved Numerical Differencing Analyzer
SPRIME -	Stay Primed subroutine to maintain evaporator in the primed state
STDSTL -	Steady-state solution routine
STUBE -	Small or short (time independent) tube
TLEN -	Tube length
UA -	Heat transfer conductance
VLL -	Vapor and liquid line thermal submodel
VOL -	Volume
XVH -	Quality of vapor (high)
XVL -	Quality of vapor (low)

APPENDIX B. CPL MODEL COMPONENT NUMBER DESIGNATIONS

This appendix matches the element numbers on the SINAPS plots with the component modeled by that element.

CPL2 FLUID SUBMODEL

PLENUM 99	Reservoir
STUBE 5	Reservoir connecting line
JUNC 10	Liquid inlet header
STUBE 2	Liquid inlet line
TANK 11	Liquid inlet line volume
CAPIL 15	Isolator wick
TANK 20	Liquid inside the evaporator pump
CAPPMP	Evaporator pump No. 4, 15 inch
JUNC 1000	Center junction
NULL 1000,2000	Inlet and outlet specialized connectors
JUNC 300	Evaporator vapor grooves
STUBE 35	Evaporator grooves
JUNC 350	Evaporator exhaust header
STUBE 65	Vapor exhaust line
TANK 4	Vapor exhaust line volume
STUBE 95	Vapor transport line
TANK 40	Vapor transport line volume
STUBE 94	Vapor inlet line to condenser
TANK 3	Condenser inlet line, condenser vapor manifold, and ½ the condenser tube volume
STUBE 93	Condenser vapor manifold
JUNC 200	Condenser inlet
HX 1-8	Condenser (One HX for each parallel condenser tube)
JUNC 100	Condenser outlet
STUBE 8	Condenser outlet line
TANK 8	Condenser outlet line, condenser liquid manifold, and ½ the condenser tube volume
CAPIL 9	NCG trap
TANK 9	NCG trap outlet line volume
STUBE 4	NCG trap outlet line
TANK 7	Liquid transport line volume
STUBE 3	Liquid transport line

CLDPLT THERMAL SUBMODEL

NODES 1-8 .... Condenser piping (Ammonia side)
NODES 9-16 .... Condenser section connector plate
NODE 999 .... Sink (Chiller) (boundary node)
COND 17-24 .... Conductance from plate to fluorinert sink
COND 25-32 .... Conductance from ammonia piping to plate

EVP SUBMODEL

NODE 600 .... Heater (arithmetic node with variable heat input)
NODE 700 .... Graphite foil (plate to plate)
NODE 800 .... Connector plate
NODE 900 .... Graphite foil (plate to bracket)
NODE 1000 .... Evaporator tube mounting bracket
NODE 1100 .... Evaporator wall
NODE 1200 .... Saturation node (arithmetic)
COND 650 .... Conductance through heater plate
COND 750 .... Contact conductance across graphite foil
COND 850 .... Conductance through connecting plate
COND 950 .... Contact conductance across graphite foil
COND 1050 .... Conductance through bracket to evaporator wall
COND 1250 .... UAevaporator
TIE 1100 .... Vapor superheat tie
TIE 1001 .... Wick back-conduction tie

VLL SUBMODEL

NODE 18 ....:... NCG outlet line
NODE 19 .... Liquid transport line
NODE 22 .... Condenser inlet line
NODE 23 .... Vapor transport line
NODE 24 .... Evaporator exhaust line
NODE 50 .... Ambient temperature (boundary node)
COND 17 .... NCG outlet line to ambient
COND 19 .... Liquid transport line to ambient
COND 22 .... Condenser outlet line to ambient
COND 23 .... Vapor transport line to ambient
COND 24 .... Evaporator exhaust line to ambient

APPENDIX C. STEADY-STATE PRESSURE PROFILES

Component Pressures (P=100W, Tcond = 0C)

— Pressure (MPa)

1. Evaporator Grooves
2. Evaporator Exhaust Header
3. Condenser Inlet
4. Condenser Outlet
5. NCG Trap Inlet
6. NCG Trap Outlet
7. Liquid Inlet Header
8. Evaporator Liquid Core

Component

Pressure (MPa)

Component Pressures (P=200W, Tcond = 0C)

Legend: —◆— Pressure (MPa)

1. Evaporator Grooves
2. Evaporator Exhaust Header
3. Condenser Inlet
4. Condenser Outlet
5. NCG Trap Inlet
6. NCG Trap Outlet
7. Liquid Inlet Header
8. Evaporator Liquid Core

X-axis: Component (0 to 8)

Y-axis: Pressure (MPa) (1.1647 to 1.1653)

Component Pressures (P=300W, Tcond = 0C)

1. Evaporator Grooves
2. Evaporator Exhaust Header
3. Condenser Inlet
4. Condenser Outlet
5. NCG Trap Inlet
6. NCG Trap Outlet
7. Liquid Inlet Header
8. Evaporator Liquid Core

Component

Pressure (MPa)

Component Pressures (P=100W, Tcond = 5C)

Legend:
- Pressure (MPa)

1. Evaporator Grooves
2. Evaporator Exhaust Header
3. Condenser Inlet
4. Condenser Outlet
5. NCG Trap Inlet
6. NCG Trap Outlet
7. Liquid Inlet Header
8. Evaporator Liquid Core

X-axis: Component (0 to 8)

Y-axis: Pressure (MPa) (1.16495 to 1.16525)

Component Pressures (P=200W, Tcond = 5C)

X-axis: Component
Y-axis: Pressure (MPa)

Legend: Pressure (MPa)

1. Evaporator Grooves
2. Evaporator Exhaust Header
3. Condenser Inlet
4. Condenser Outlet
5. NCG Trap Inlet
6. NCG Trap Outlet
7. Liquid Inlet Header
8. Evaporator Liquid Core

Component Pressures (P=300W, Tcond = 5C)

1. Evaporator Grooves
2. Evaporator Exhaust Header
3. Condenser Inlet
4. Condenser Outlet
5. NCG Trap Inlet
6. NCG Trap Outlet
7. Liquid Inlet Header
8. Evaporator Liquid Core

Pressure (MPa)

Component

APPENDIX D. STEADY-STATE TEMPERATURE COMPARISONS

System Temp. Profile (Q=100W, Cond=0C)

Legend:
- MODEL
- TEST

1. Evaporator (Vapor Grooves)
2. Evaporator Vapor Header
3.,4. Vapor Transport Line
5. Condenser Inlet
6. Condenser Tube (entrance)
7. Condenser Tube (exit)
8. Condenser exit
9. NCG Entrance
10. NCG Outlet
11. Liquid Transport Line
12. Liquid Inlet Header
13. Evaporator Liquid Core

X-axis: Component

Y-axis: Temperature (C)

System Temp. Profile (Q=200W, Cond=0C)

Legend:
- MODEL
- TEST

X-axis: Component
Y-axis: Temperature (C)

1. Evaporator (Vapor Grooves)
2. Evaporator Vapor Header
3.,4. Vapor Transport Line
5. Condenser Inlet
6. Condenser Tube (entrance)
7. Condenser Tube (exit)
8. Condenser exit
9. NCG Entrance
10. NCG Outlet
11. Liquid Transport Line
12. Liquid Inlet Header
13. Evaporator Liquid Core

System Temp. Profile (Q=300W, Cond=0C)

Legend:
- MODEL
- TEST

#	Component
1.	Evaporator (Vapor Grooves)
2.	Evaporator Vapor Header
3.,4.	Vapor Transport Line
5.	Condenser Inlet
6.	Condenser Tube (entrance)
7.	Condenser Tube (exit)
8.	Condenser exit
9.	NCG Entrance
10.	NCG Outlet
11.	Liquid Transport Line
12.	Liquid Inlet Header
13.	Evaporator Liquid Core

X-axis: Component
Y-axis: Temperature (C)

System Temp. Profile (Q=100W, Cond=5C)

Legend: MODEL, TEST

1.	Evaporator (Vapor Grooves)
2.	Evaporator Vapor Header
3.,4.	Vapor Transport Line
5.	Condenser Inlet
6.	Condenser Tube (entrance)
7.	Condenser Tube (exit)
8.	Condenser exit
9.	NCG Entrance
10.	NCG Outlet
11.	Liquid Transport Line
12.	Liquid Inlet Header
13.	Evaporator Liquid Core

X-axis: Component

Y-axis: Temperature (C)

System Temp. Profile (Q=200W, Cond=5C)

Legend:
- MODEL
- TEST

1. Evaporator (Vapor Grooves)
2. Evaporator Vapor Header
3.,4. Vapor Transport Line
5. Condenser Inlet
6. Condenser Tube (entrance)
7. Condenser Tube (exit)
8. Condenser exit
9. NCG Entrance
10. NCG Outlet
11. Liquid Transport Line
12. Liquid Inlet Header
13. Evaporator Liquid Core

Temperature (C)

Component

System Temp. Profile (Q=300W, Cond=5C)

1.	Evaporator (Vapor Grooves)
2.	Evaporator Vapor Header
3.,4.	Vapor Transport Line
5.	Condenser Inlet
6.	Condenser Tube (entrance)
7.	Condenser Tube (exit)
8.	Condenser exit
9.	NCG Entrance
10.	NCG Outlet
11.	Liquid Transport Line
12.	Liquid Inlet Header
13.	Evaporator Liquid Core

Legend: MODEL, TEST

X-axis: Component (0 to 14)
Y-axis: Temperature (C) (5 to 35)

APPENDIX E. TRANSIENT SIMULATION RESULTS

System Temperatures (Power Change 300-50W)

Black = Vapor Grooves   Green = Liquid Header
Pink = Vapor Header   Light Blue = NCG Outlet
Dark Blue = Evaporator Liquid Core

Temperature (C)

Time (seconds)

106
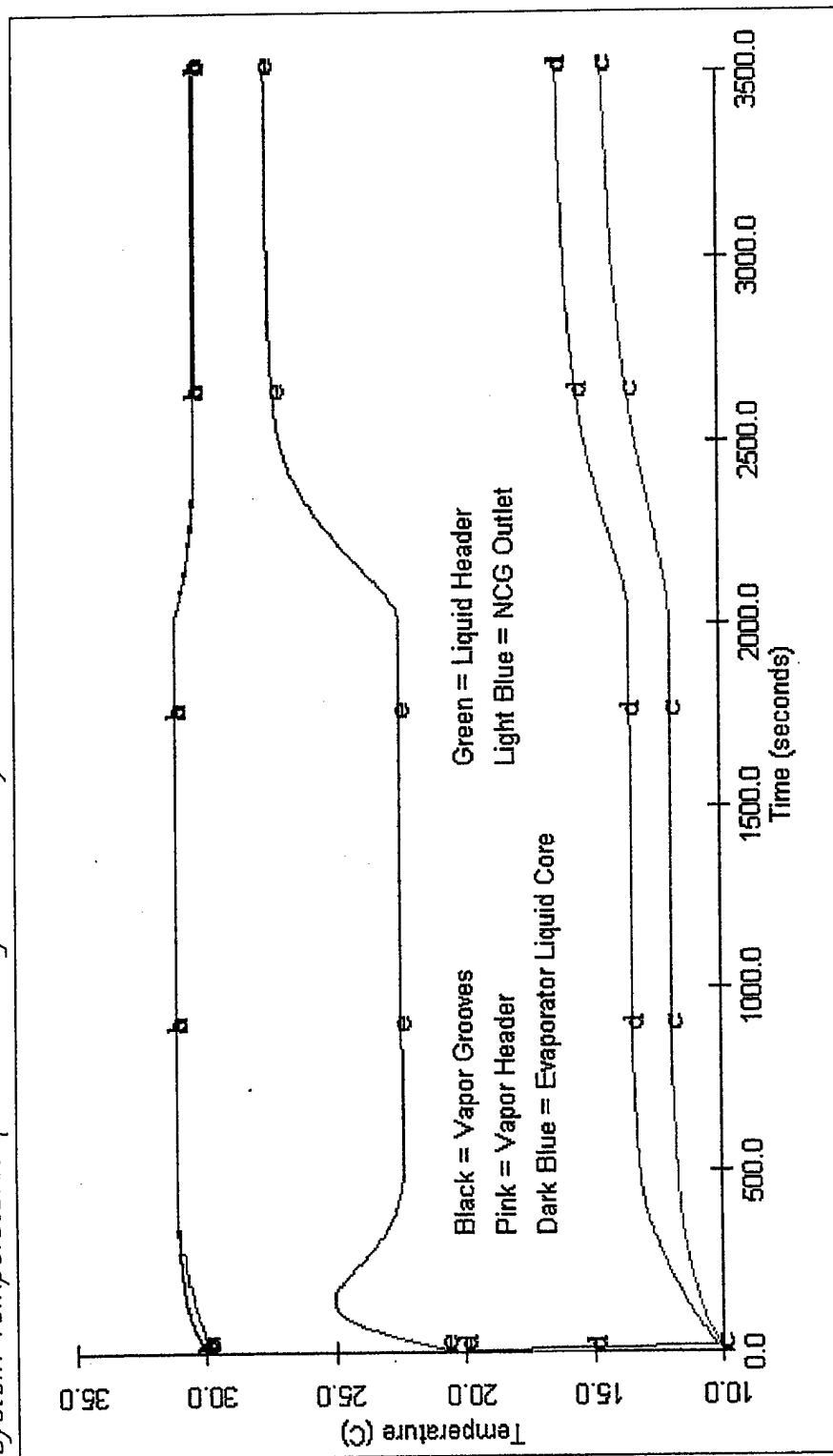
System MFR (Condenser Temperature Changes)
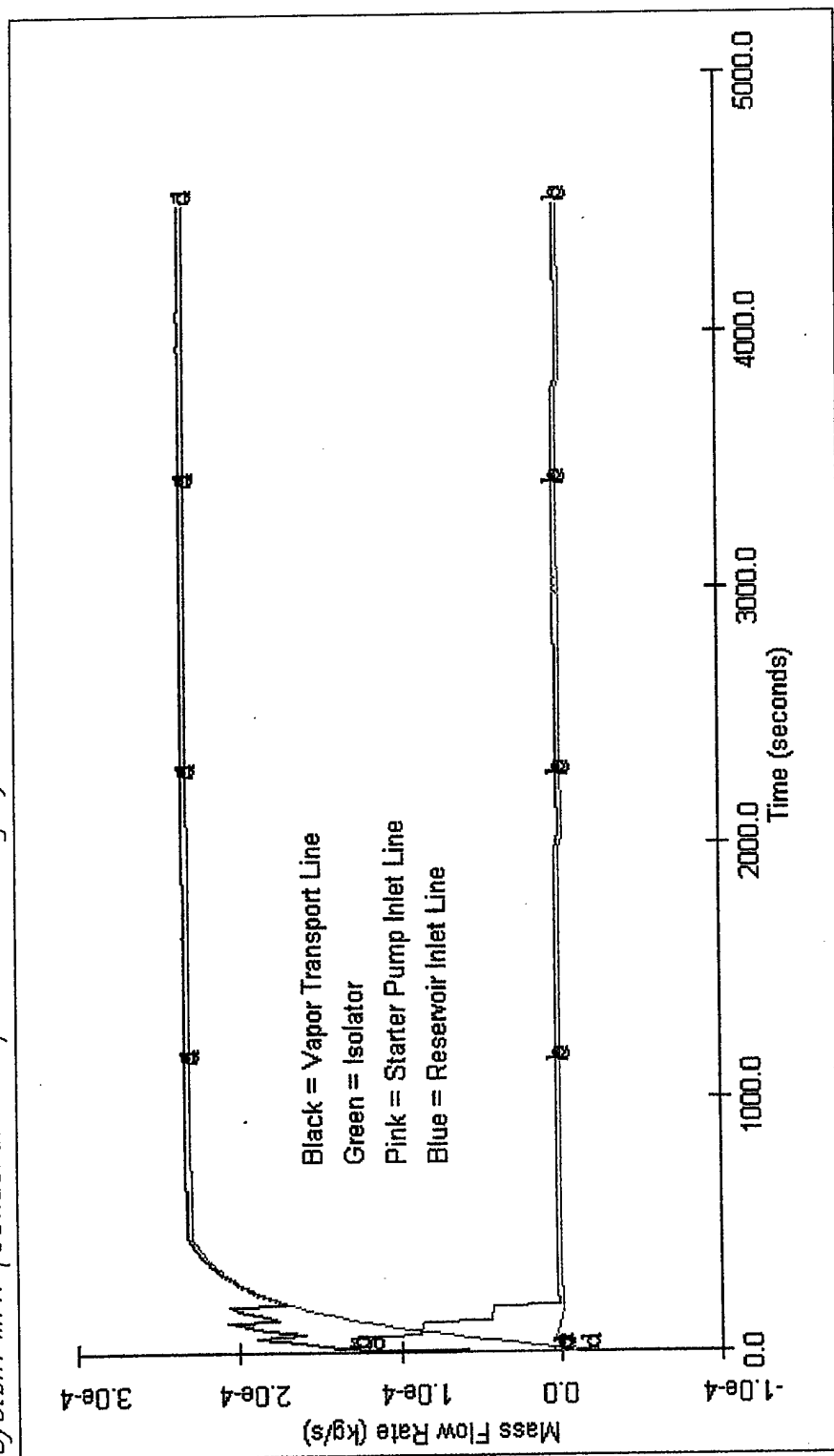
System Temperatures (Condenser Temperature Changes)

Black = Vapor Grooves   Green = Liquid Header

Pink = Vapor Header   Light Blue = NCG Outlet

Dark Blue = Evaporator Liquid Core

Time (seconds)

Temperature (C)

108
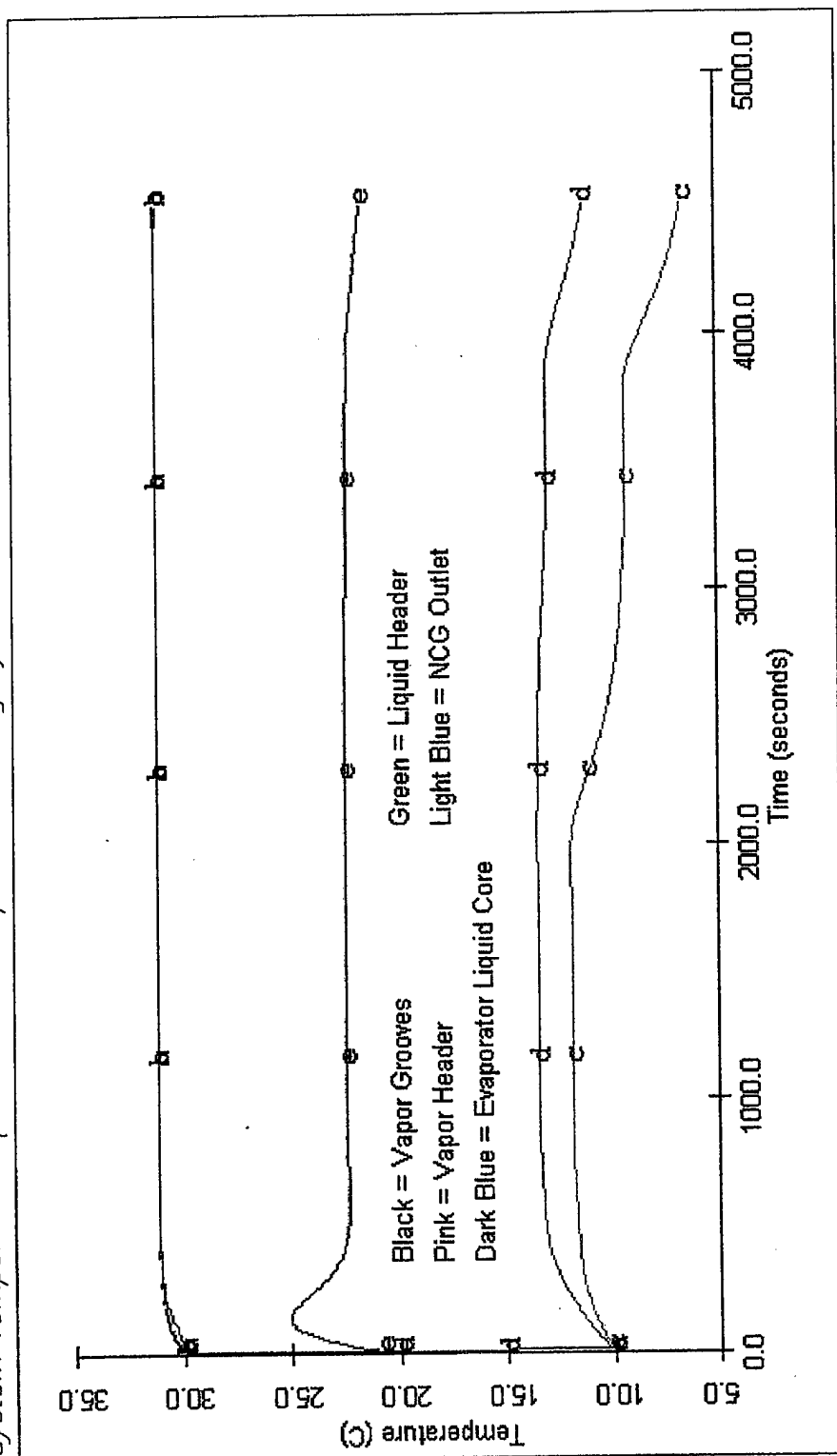
Condenser Quality (Condenser Temperature Changes)

'a' through 'j' represent junctions in the condenser, with 'a' being closest to the inlet and 'j' closest to the outlet

System MFR (Power Change 200-300-100W)

Black = Vapor Transport Line
Green = Isolator
Pink = Starter Pump Inlet Line
Blue = Reservoir Inlet Line

System Temperatures (Power Change 200-300-100W)

Black = Vapor Grooves
Pink = Vapor Header
Dark Blue = Evaporator Liquid Core

Green = Liquid Header
Light Blue = NCG Outlet

Temperature (C)

Time (seconds)

Condenser Quality (Power Change 200-300-100W)

'a' through 'j' represent junctions in the condenser, with 'a' being closest to the inlet and 'j' closest to the outlet

System MFR (Power Change 200-100W)

Black = Vapor Header
Green = Isolator
Pink = Starter Pump Inlet Line
Blue = Reservoir Inlet Line

Mass Flow Rate (kg/s)

Time (seconds)

System Temperatures (Power Change 200-100W)

Black = Vapor Grooves   Green = Liquid Header

Pink = Vapor Header   Light Blue = NCG Outlet

Dark Blue = Evaporator Liquid Core

Temperature (C)

Time (seconds)

114

Condenser Quality (Power Change 200–100W)

'a' through 'j' represent junctions in
the condenser, with 'a' being closest
to the inlet and 'j' closest to the
outlet

Quality

Time (seconds)

115

System MFR (Power Change 50-300W, Cond. = 15C)

Black = Vapor Header
Green = Isolator
Pink = Starter Pump Inlet Line
Blue = Reservoir Inlet Line

Mass Flow Rate (kg/s)

Time (seconds)

116

System Temperatures (Power Change 50-300W, Cond. = 15C)

Black = Vapor Grooves
Pink = Vapor Header
Dark Blue = Evaporator Liquid Core
Green = Liquid Header
Light Blue = NCG Outlet

Time (seconds)

Temperature (C)

Condenser Quality (Power Change 50-300W. Cond. = 15C)

'a' through 'j' represent junctions in the condenser, with 'a' being closest to the inlet and 'j' closest to the outlet

118

APPENDIX F. TEMPERATURE-TIME COMPARISONS

Liquid Line Temperature Profile
(Power Change 200-300W)

Legend:
- Test
- Model

X-axis: Time (s) — 3820, 4000, 4020, 4040, 4060, 4080, 4100, 4120, 4140, 4160, 4180, 4200, 4220, 4240, 4260, 4280, 4300, 4320, 4450, 4690

Y-axis: Temperature (C) — 1.00E+01, 1.10E+01, 1.20E+01, 1.30E+01, 1.40E+01, 1.50E+01, 1.60E+01, 1.70E+01, 1.80E+01, 1.90E+01, 2.00E+01

120
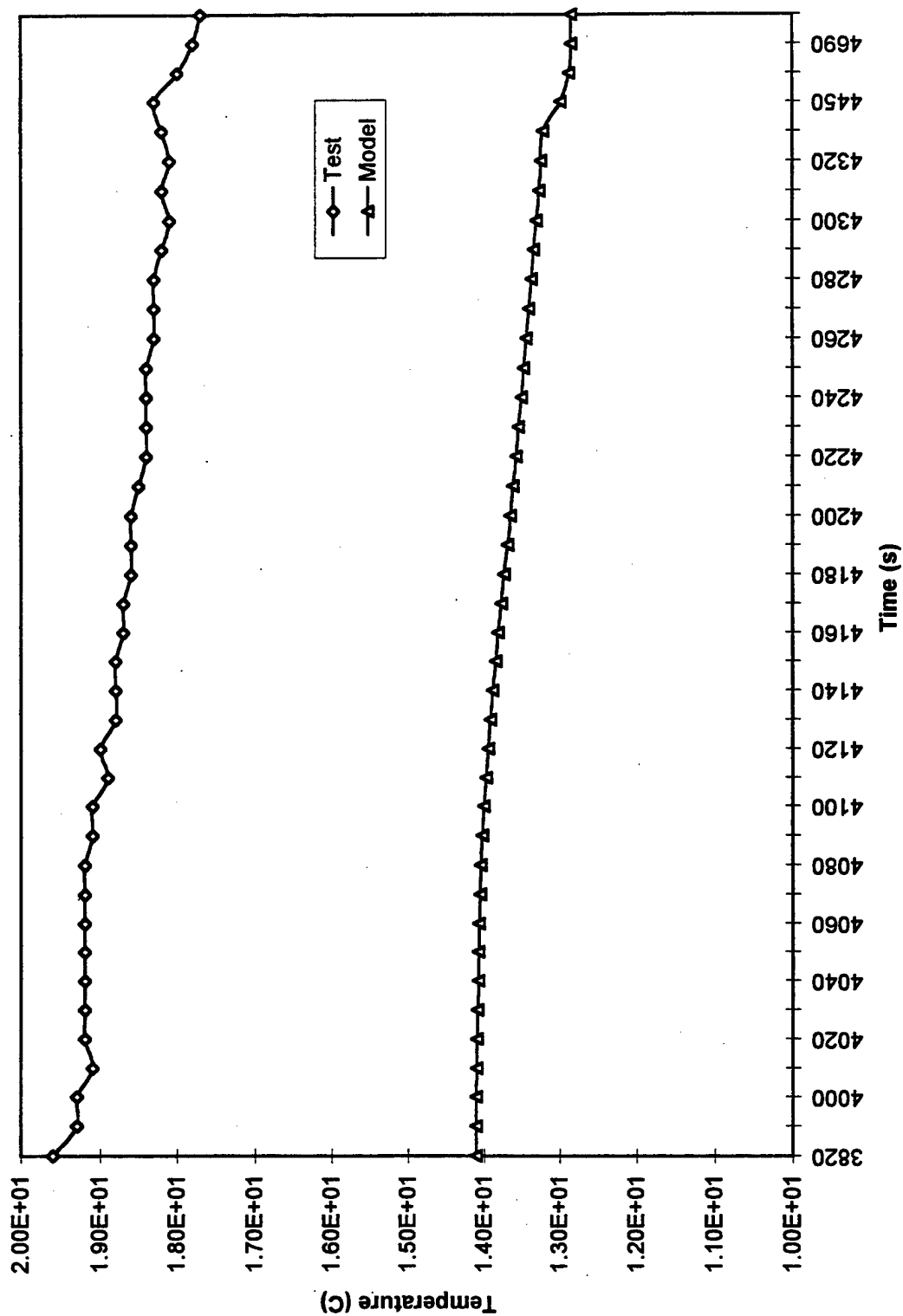
Evaporator Liquid Core Temperature Profile
(Power Change (200-300W))

121
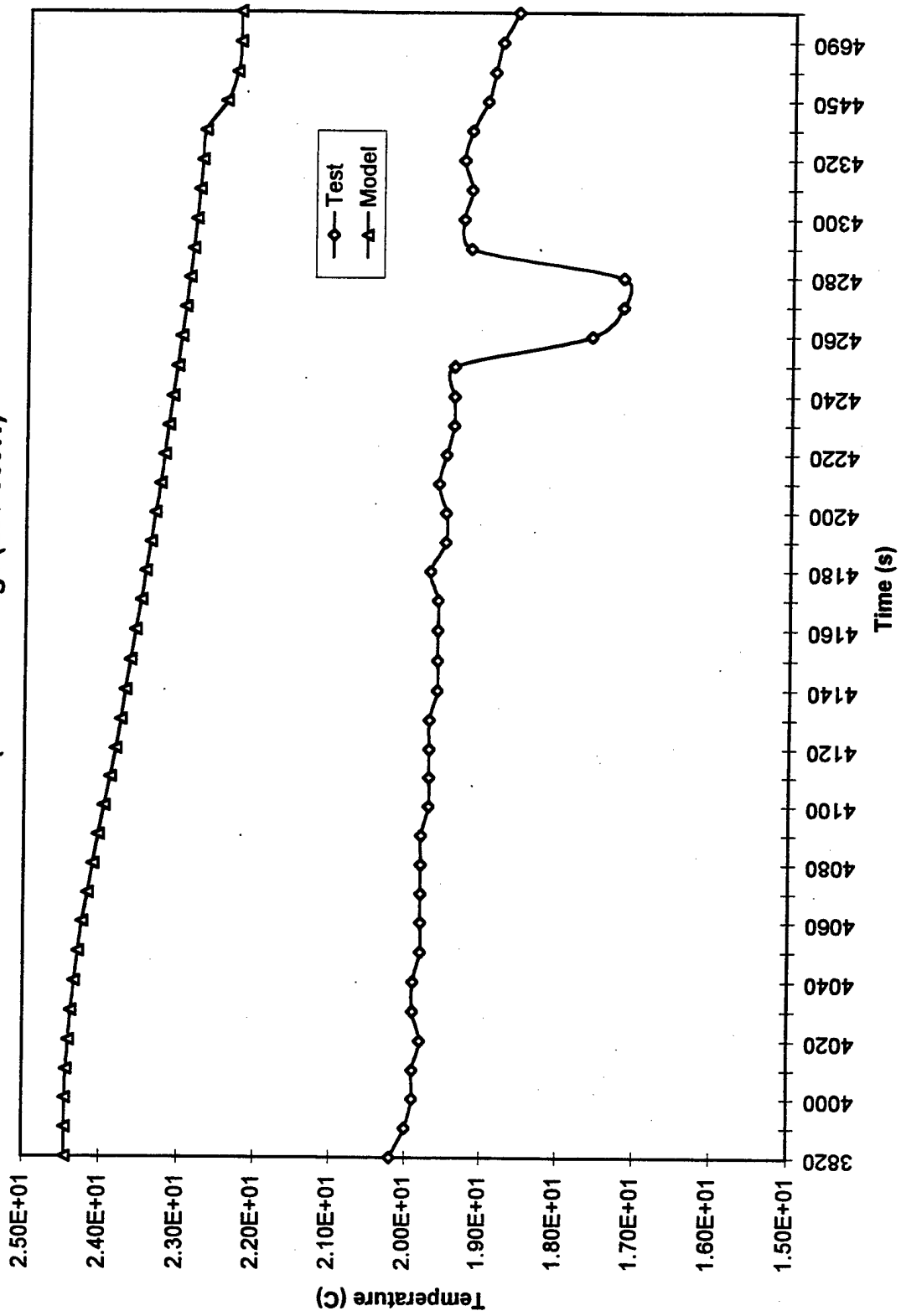
Condenser Outlet Temperature Profile
(Power Change 200-300W)
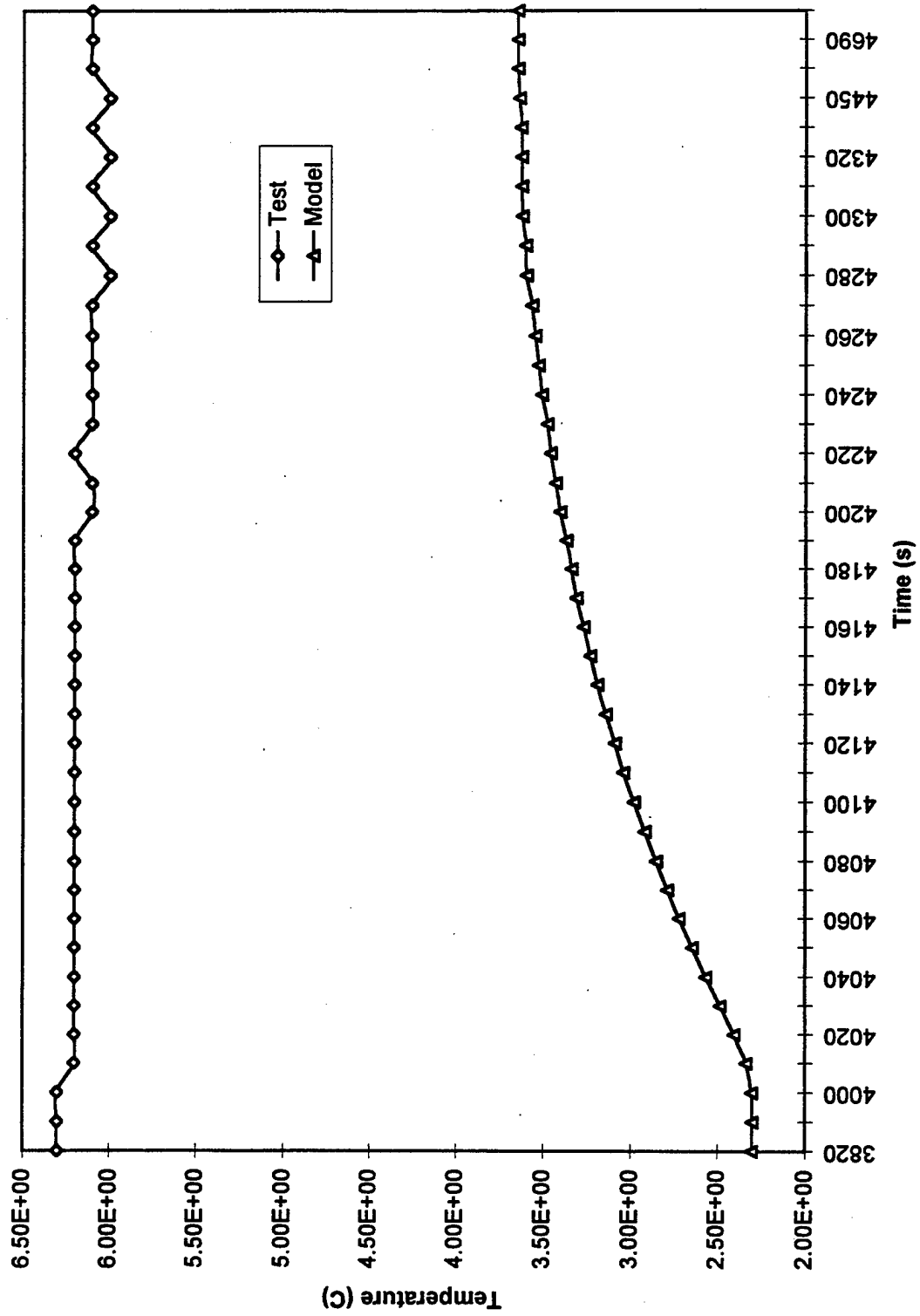
LIST OF REFERENCES

1. Larson, Wiley J. and Wertz, James R., *Space Mission Analysis and Design*, Microcosm, Inc., Torrence, CA, 1992.

2. Gilmore, David G., *Satellite Thermal Control Handbook*, Aerospace Corporation Press, El Segundo, CA, 1994.

3. Cullimore, Brent A., *Capillary Pumped Loop Application Guide*, Martin Marietta Group, Denver, CO, 1993.

4. Silverstein, Calvin C., *Design and Technology of Heat Pipes for Cooling and Heat Exchange*, Taylor & Francis, Washington, D.C., 1992.

5. Peterson, G. P., *An Introduction to Heat Pipes: Modeling, Testing, and Applications*, John Wiley & Sons, Inc., New York, 1994.

6. Maidanik, Y., Fershtater, Y., and K. Goncharov, *Capillary Pump Loop for the System of Thermal Regulation of Spacecraft*, European Symposium on Space Environmental and Control Systems, 1991.

7. Kiseev, V. M. *Analysis of Maximum Heat Transfer Capacity of Capillary Loops*, Ural State University, Russia, 1995.

8. *Solar Cell Array Design Handbook*, Volume 152, NASA/JPL Publication SP 43-38.

9. *Test Plan for the Capillary Pumped Loop (CPL) Test Bed*, U.S. Air Force Phillips Laboratory Power and Thermal Management Division (PL/VTPT), Kirtland AFB, Albuquerque, NM. 1995.

10. Stenger, F. J., *Experimental Feasibility Study of Water-Filled Capillary Pumped Heat-Transfer Loops*, NASA TM-X-1310, NASA Lewis Research Center, Cleveland, OH., 1966.

11. Yun, S., Nguyen, T., Kroliczek, E., Chalmers, D., and J. Fredley, *Design and Ambient Testing of the Flight Starter Pump Cold Plate*, SAE ICES Conference, Monterey, CA, 1996.

12. Meyer, R., Muller, R., Beckmann, K., Goncharov, K., Kotlarov, E., and Maidanik, Y., *Investigation of the Heat Transfer Performance of a Capillary Pumped Ammonia Loop Under Gravity*, SAE ICES Conference, Colorado Springs, CO, 1993.

13. Ku, Jentung, *Overview of Capillary Pumped Loop Technology*, NASA Goddard Space Flight Center, Greenbelt, MD, 1994.

14. Baumann, J., *Recommendations for Future CPL Development and Risk Reduction*, Martin Marietta Astronautics Group, Denver, CO, 1993.

15. Baumann, J., *Advances in CPL Technology*, CPL Workshop III, Sponsored by NASA Goddard Space Flight Center, Annapolis, MD, 1992.

16. Cullimore, B., et al, *SINDA/FLUINT Version 3.2 User's Manual*, September 1994.

17. Kuntz, Robert J., "Where is Rachel", *Launchspace Magazine*, March 1997.

18.   White, Frank M. *Fluid Mechanics, Third Ed.* McGraw-Hill, San Francisco, 1994.

INITIAL DISTRIBUTION LIST

1. Defense Technical Information Center 2
   8725 John J. Kingman Road, Ste 0944
   Ft. Belvoir, Virginia 22060-6218

2. Dudley Knox Library 2
   Naval Postgraduate School
   411 Dyer Road
   Monterey, California 93943-5101

3. Naval/Mechanical Engineering Curricular Officer, Code 34 1
   Naval Postgraduate School
   Monterey, California 93943-5101

4. Mechanical Engineering Department Chairman, Code ME 1
   Naval Postgraduate School
   Monterey, California 93943-5101

5. Professor Matthew D. Kelleher 3
   Mechanical Engineering Department, Code ME/KK
   Naval Postgraduate School
   Monterey, California 93943-5101

6. Dr. Donald Gluck 3
   Phillips Laboratory, VTPT
   3550 Aberdeen Ave., S.E.
   Building 30117
   Kirtland AFB, NM 87117-5776

7. LT Peter J. Ryan, Jr., USN...1
   11338 S.E. 175th Place
   Summerfield, Florida 34491

8. Brent Cullimore..1
   Cullimore and Ring Technologies
   9 Red Fox Lane
   Littleton, CO 80127

9. Dr. Rudolph Panholzer 1
   Chairman, Space Systems Academic Group
   Code SP/PZ
   Naval Postgraduate School
   Monterey, CA 93943-5002